

Experimental determination of the thermal, turbulent, and rotational ion motion and magnetic field profiles in imploding plasmas

F

Cite as: Phys. Plasmas **27**, 060901 (2020); <https://doi.org/10.1063/5.0009432>

Submitted: 30 March 2020 . Accepted: 04 June 2020 . Published Online: 26 June 2020

Yitzhak Maron 

COLLECTIONS

Note: This paper is part of the Special Collection: Papers from the 61st Annual Meeting of the APS Division of Plasma Physics. Note: Paper PT3 1, Bull. Am. Phys. Soc. 64 (2019).

 This paper was selected as Featured



View Online



Export Citation



CrossMark

ARTICLES YOU MAY BE INTERESTED IN

[A conservative approach to scaling magneto-inertial fusion concepts to larger pulsed-power drivers](#)

Physics of Plasmas **27**, 062707 (2020); <https://doi.org/10.1063/1.5135716>

[Magnetic field impact on the laser heating in MagLIF](#)

Physics of Plasmas **27**, 052704 (2020); <https://doi.org/10.1063/1.5129417>

[Hotspot conditions achieved in inertial confinement fusion experiments on the National Ignition Facility](#)

Physics of Plasmas **27**, 050901 (2020); <https://doi.org/10.1063/5.0003298>



NEW: TOPIC ALERTS

Explore the latest discoveries in your field of research

SIGN UP TODAY!



Experimental determination of the thermal, turbulent, and rotational ion motion and magnetic field profiles in imploding plasmas

Cite as: Phys. Plasmas **27**, 060901 (2020); doi: [10.1063/5.0009432](https://doi.org/10.1063/5.0009432)

Submitted: 30 March 2020 · Accepted: 4 June 2020 ·

Published Online: 26 June 2020



View Online



Export Citation



CrossMark

Yitzhak Maron ^{a),b)} 

AFFILIATIONS

Faculty of Physics, Weizmann Institute of Science, Rehovot 7610001, Israel

Note: This paper is part of the Special Collection: Papers from the 61st Annual Meeting of the APS Division of Plasma Physics.

Note: Paper PT31, Bull. Am. Phys. Soc. **64** (2019).

^{a)}Invited speaker.

^{b)}Author to whom correspondence should be addressed: yitzhak.maron@weizmann.ac.il

ABSTRACT

A tutorial is presented on advances in spectroscopic diagnostic methods developed for measuring key plasma properties in pulsed-power systems such as Z-pinches, magnetized-plasma compression devices, ion and electron diodes, and plasma switches. The parameters measured include the true ion temperature in Z-pinch implosions, which led to a discovery that much of the ion kinetic energy at stagnation is stored in hydrodynamic rather than in thermal motion. This observation contributed a new important insight into the understanding of the ion thermalization at stagnation and stimulated further investigations of turbulence at stagnation, discussed here too. The second part of this tutorial is devoted to the development of measurements for magnetic-field distributions in Z-pinches and in other pulsed-power systems, as well as their use in studying the plasma dynamics, resistivity, and pressure and energy balance. The latter study raises intriguing questions on the implosion process. In particular, in Z-pinches, the current during stagnation was found to largely flow at relatively large radii, outside the stagnation region. The magnetic-field measurements also enable investigations into the compression of a pre-magnetized cylindrical plasma that uncover striking phenomena related to the current flow, where the current was found to redistribute toward the outer regions during the implosion. Observation of the rotation of the magnetized plasma is also discussed. Finally, experimental and theoretical investigations of a non-diffusive fast penetration of magnetic field into a low-density plasma, including its effect on the plasma dynamics, are described.

Published under license by AIP Publishing. <https://doi.org/10.1063/5.0009432>

I. INTRODUCTION

Improving the fundamental understanding of processes governing the behavior of high-energy-density (HED) plasmas formed under intense pulses of current or radiation is essential for the research of numerous laboratory^{1–6} and astrophysical plasmas.^{7–9} However, progress in the diagnostics of such plasmas is rather challenging due to the inherent irreproducibility of the experiments, the limited access, the 3D nature of the phenomena involved, the development of instabilities in the plasma, and the complexity of the theoretical models. In particular, for spectroscopic diagnostics, which is often the only way to probe into HED plasmas, challenges are imposed due to various atomic processes that take place simultaneously in a strongly non-equilibrium plasma state, nonuniformities of the plasmas, and the imposed integration along the lines of view. In addition, the spectra emitted or absorbed by the plasmas are affected by a variety of factors,

such as Stark broadening and shift, Zeeman splitting, Doppler broadening and shift, opacity, and the presence of charge states with multiply excited levels.

This tutorial describes the progress in measuring key plasma properties in a variety of pulsed-power systems and the impact of these measurements on advancing our understanding of the physics in these systems. We begin with measurements by Kroupp *et al.*^{10,11} that demonstrated, unlike the earlier common belief, that the ion kinetic energy at the Z-pinch stagnation is dominated by hydromotion rather than by the temperature. This observation is of fundamental importance, since it is the true ion temperature that decisively affects the applications, whether they are radiation sources,^{12–16} neutron sources,^{16,17} pinch-driven hohlraums,⁴ or radiation-driven implosions^{18,19} for inertial confinement fusion (ICF). In the measurements,^{10,11} the thermal motion and hydromotion were discriminated, including the

determination of the dissipation time of the latter. Also presented is a new method, recently developed by Alumot *et al.*,²⁰ that yields the ion temperature in HED plasmas in a profoundly explicit way, based on sensitivity of the spectral shapes of certain Stark-broadened emission lines to the ion temperature. It is believed that this method is applicable in various HED plasma experiments.

One of the fundamental questions of plasma dynamics is the pressure and energy balance, including contributions of the magnetic field due to the currents flowing through the plasma. We discuss here the use of the Zeeman effect for determining time-dependent magnetic-field distributions in pulsed-power systems, namely Z-pinch implosions, compressing magnetized plasmas, ion and electron diodes, and plasma opening switches (POS). The magnetic-field measurements described encompass plasma density in the range of 10^{14} – 10^{19} cm⁻³.

For the Z-pinch implosions, unexpected findings on the time-dependent radial distribution of the magnetic field at stagnation are presented. Furthermore, an unexpected redistribution of the axial current during the compression of magnetized plasma is described, together with a discussion on the plasma rotation in such a configuration. In addition, the use of the magnetic field measurements in determining the plasma resistivity in the various systems is presented.

Non-diffusive fast magnetic field penetration into the plasma has been observed in plasma opening switches (see, for example, Refs. 21–24) using spectroscopic diagnostics augmented by doping techniques.^{25–34} Described are spectroscopic measurements that reveal the details of the magnetic field evolution and plasma dynamics during the field penetration. The field penetration with the accompanying ion separation²⁸ was found to result from nonuniformities in the lower-density plasmas that made the Hall electric field dominant.

II. DETERMINATION OF THE ION TEMPERATURE IN A STAGNATING Z-PINCH PLASMA BASED ON ENERGY BALANCE

Both wire-array and gas-puff Z-pinches have been employed for a few decades in controlled fusion^{2,4,35} and development of radiation sources.^{1,12–16,36,37} The interest in fusion using Z-pinches has evolved into complex designs for the pulsed-power load that require at least 2D magnetohydrodynamic (MHD) simulations; a recent example of such a modeling can be seen in the study by Slutz³⁸ for the Magnetized Liner Inertial Fusion (MagLIF) concept.^{3,39} As radiation sources, Z-pinches have mainly been used to obtain intense x-ray pulses from atoms ionized into the K-shell,^{12–16,35} which require a detailed treatment of non-LTE (local thermodynamic equilibrium) ionization kinetics and radiation transfer, see, for example, Fisher *et al.*,⁴⁰ Scott and Hansen,⁴¹ and Thornhill *et al.*⁴² The implosion phase of Z-pinches is particularly subject to the magneto-Rayleigh–Taylor instability because a light fluid, i.e., the vacuum magnetic field, is accelerating a heavy fluid, i.e., the material load. The instability is captured by resistive 3D MHD simulations as shown by Chittenden and Jennings⁴³ and Jennings *et al.*⁴⁴

It was commonly believed^{1,16,36} that the ions accelerated in the imploding plasma rapidly thermalize at stagnation (at the ion–ion collision time τ_{ii}), so that the entire ion kinetic energy at stagnation rapidly becomes thermal. Then, the ions deliver their thermal energy to the electrons (at the time scale τ_{ie} of the ion–energy loss to the electrons), followed by the loss of the electron heat through ionization and excitation to radiation. Indeed, in experiments, the Doppler

broadening of line emission from the stagnated plasma was used to infer the ion temperature, assuming that the total broadening reflects the ion thermal motion.^{45–48}

However, detailed energy balance considerations,^{10,11} enabled by time-resolved, local measurements of multiple parameters in a stagnating Z-pinch plasma, allowed for the discovery that a large fraction of the ion kinetic energy in such a plasma is hydrodynamic rather than thermal. This study, performed on an implosion of a neon-puff plasma, see Fig. 1, yielded the time-dependent total ion kinetic energy along the pinch column, obtained from the Doppler broadening of an optically thin spectral line. To obtain this information, an imaging spherical crystal with a resolving power of ~ 6700 had to be used. The electron density was determined from the ratio of triplet-satellite lines^{10,11,49} and the electron temperature from neon K-line ratios,^{10,50} using collisional-radiative computations developed by Ralchenko and Maron.⁵¹ In addition, the total radiation emitted from a specific segment along the pinch column, and the pinch structure with a spatial resolution of ~ 100 μm , were determined from x-ray radiation power and x-ray imaging, respectively.

In the experiment, the ion Doppler pseudo-temperature T_i^D was obtained from the FWHM of the singlet-satellite shape, where $3/2 T_i^D$ is defined to give the total ion kinetic energy E_k^{total} , i.e.,

$$\frac{3}{2} T_i^D = E_k^{total} = \frac{3}{2} T_i + E_k^{hydro}. \quad (1)$$

Here, T_i is the true ion temperature and E_k^{hydro} is the ion kinetic energy in the hydrodynamic motion. In the data, T_i^D was seen to drop from 4 to 5 keV early at stagnation to about the electron temperature T_e (~ 200 eV) at the end of the stagnation, as shown in Fig. 2. It was also shown,^{10,11} by the use of radiation-transport computations due to Fisher *et al.*,⁴⁰ that the observed drop in $3/2 T_i^D$, multiplied by the number of ions in the stagnating plasma, explains the total radiation emitted, i.e., the dissipation of E_k^{total} explains the energy required for the total radiation measured. It should also be emphasized that the total radiation was spatially resolved, so that $3/2 T_i^D$ and the total radiation emission were compared locally for a specific region along the pinch column.

Assuming the only way for electrons in the plasma to obtain heat (and eventually to deposit it into radiation emission) is from the ions, the data analysis allowed for inferring an upper limit for the true ion temperature by using the following equation:

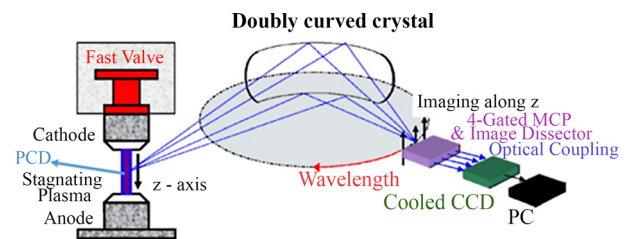


FIG. 1. Schematic of the diagnostic setup: a doubly curved potassium acid phthalate (KAP) crystal (second order) system, with a spectral resolving power of ~ 6700 , coupled to a time resolved detector, capable of recording four x-ray images 1 ns apart in a single discharge. The spectrum from the stagnating plasma is 1D-imaged along z , with a spatial resolution of ~ 100 μm . A photoconducting device (PCD) is used to measure the power of the entire radiation above ≈ 700 eV, from a region 2 mm long in the z direction and centered at $z = 5$ mm ($z = 0$ is the cathode surface), from which all other spectroscopic data discussed above are collected.

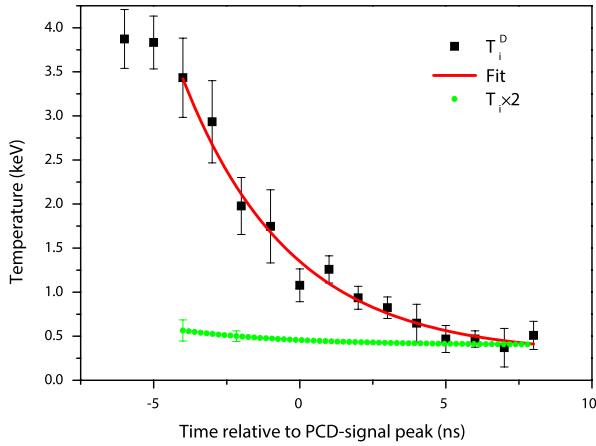


FIG. 2. The measured ion Doppler pseudo-temperature T_i^D (black dots) as a function of time throughout a neon-puff stagnation, obtained from the measured shape of the singlet Ly- α satellite. $t=0$ denotes the time of peak radiation power measured by the PCD (see Fig. 1). Also shown is the true ion temperature (green line), obtained from the fit to T_i^D using Eq. (3), with the uncertainty shown by the bars. Each data point is an average over 2–5 identical discharges. The stagnating plasma parameters are $n_e \approx 6 \times 10^{20} \text{ cm}^{-3}$, $T_e \approx 200 \text{ eV}$, and $\bar{Z} = 9$. Reproduced from Kroupp *et al.*, Phys. Rev. Lett. **107**, 105001 (2011).¹¹ Copyright 2011 American Physical Society.

$$\frac{dT_i}{dt} = -\frac{T_i - T_e}{\tau_{ie}} - \frac{2}{3} \frac{dE_k^{hydro}}{dt}. \quad (2)$$

The negative value of the time derivative of the kinetic energy of the hydromotion indicates dissipation of the hydromotion into ion heat (followed by the ion-heat dissipation into electron heating). Using (1) and (2), we obtain

$$\frac{dT_i^D}{dt} = -\frac{T_i - T_e}{\tau_{ie}}. \quad (3)$$

Thus, the measured drop in time of $T_i^D(t)$ was used to determine $T_i(t)$, with $\tau_{ie} \sim 0.1 \text{ ns}$, inferred from the values determined for T_e ($\sim 200 \text{ eV}$), n_e ($\sim 6 \times 10^{20} \text{ cm}^{-3}$), and $\bar{Z} = 9$. As seen in Fig. 2, the true ion temperature was found to be much lower than the total ion kinetic energy at the beginning of the stagnation, staying at a relatively low value, close to the electron temperature, up to the end of stagnation.

We note that Eq. (3) implies that the entire E_k^{hydro} dissipates into ion heating, which is justified by the finding (mentioned above) that the total radiation output is explained by the loss of E_k^{total} in the plasma. It should be emphasized, however, that if part of E_k^{hydro} is not dissipated into ion heating, the true T_i would even be lower. In addition, in principle, electrons could be heated by mechanisms other than heating by the ions, as was discussed in Refs. 47 and 52–57, considering Ohmic heating or dissipation of magnetic-field energy at the stagnation. This would mean less electron heating by ions (otherwise, the total radiation would exceed the measured value), i.e., the true ion temperature should even be lower than given in Fig. 2. It should also be pointed out that the upper limit of T_i determined in Ref. 11 reflects the true T_i in the stagnating plasma, since its determination is based on H-like transitions that are only emitted from the stagnating plasma,

i.e., not affected by emission from the radially flowing imploding plasma. Note that since in Eq. (3) used is the time derivative of the instantaneous T_i^D spatially averaged over the stagnating plasma, the average $(T_i - T_e)$ obtained is non-dependent neither on the fact that particles of the imploding plasma flow into the stagnation region at different times (and thus have less time to dissipate their hydro-energy) nor on possible variations in the imploding plasma velocity throughout the stagnation period. As a final comment, the true ion temperature T_i , as seen in Eq. (3), is determined by the relative rates of the hydromotion dissipation and the ion heat loss to electrons. The finding that $T_i \ll T_i^D$ throughout most of the stagnation is an outcome of the slow dissipation rate (a few ns, see Fig. 2) observed for E_k^{hydro} relative to the rate of ion-heat loss to electrons. Obviously, for both fusion and the production of intense radiation sources, a fast dissipation of E_k^{hydro} into ion heating is required. However, for fusion, a slow ion-electron energy transfer is crucial, while for intense radiation pulses, a fast ion-electron energy transfer is demanded, at least as fast as the dissipation of E_k^{hydro} .

III. IMPLICATIONS OF THE T_i MEASUREMENTS TO Z-PINCH PHYSICS

A. Use of the stagnation studies for evaluating the pressure and energy balance and the current flow in the stagnating plasma

The most fundamental questions of the Z-pinch stagnation dynamics are the plasma heating mechanisms and the energy and pressure balance in the plasma. It is of particular importance to understand the contribution of the magnetic field to the pressure balance at the stagnating plasma and the fraction of current flowing there. It was commonly believed^{1,16,47,57–60} that the magnetic field determines the pressure balance in the stagnating plasma. In particular, the Bennett relation,⁶¹ i.e., the balance between the magnetic and thermal pressures, along with the related assumption (e.g., Refs. 47, 53, and 55) that most of the current in the imploding plasma flows through the stagnation region, was assumed. It was also widely believed that the B-field energy at stagnation plays an important role in the energy dissipation and growth of instabilities there.^{47,52–57,59,62} Furthermore, some studies pointed out that the total energy radiated from the pinch might exceed the kinetic energy of the implosion.^{47,53–56,62,63}

The spectroscopic measurements presented in Refs. 10 and 11 for the gas-puff experiment, with the relatively low-power system (current pulse of 500 kA over 500 ns), were used to investigate the pressure and energy balance at stagnation.⁶⁴ Also analyzed for this work were data from an experiment of notably different parameters described by Coverdale *et al.*,⁶⁵ namely, a nested wire-array implosion on the Z facility,^{4,12,66} with a current pulse of $\sim 20 \text{ MA}$ over $\sim 100 \text{ ns}$. The plasma properties found were examined within a 1D shock wave picture following the relations between the imploding and stagnating plasma properties:

$$\frac{n_2}{n_1} = \frac{v_1}{v_2}, \quad (4)$$

$$\frac{n_2}{n_1} = \frac{mv_1^2 + T_{i1}^D + Z_1 T_{e1}}{mv_2^2 + T_{i2}^D + Z_2 T_{e2}}, \quad (5)$$

$$\frac{mv_1^2}{2} = \frac{mv_2^2}{2} + \Delta\epsilon_{ion} + \delta_{rad} + \frac{5}{2} [T_{i2}^D + Z_2 T_{e2} - (T_{i1}^D + Z_1 T_{e1})], \quad (6)$$

where m , n , and v are the ion mass, density, and directed particle velocity, respectively, $\Delta\epsilon_{ion}$ is the change in the internal ionization energy per ion across the shock, δ_{rad} is the average total radiation per ion emitted from the shocked plasma up to the peak of the K-radiation emission, and the pressure $P = n(T_i^D + ZT_e)$, where for the ion pressure the ion Doppler pseudo-temperature T_i^D was used, i.e., including the hydromotion energy, see e.g., Ref. 67. The regions of the leading edge of the imploding and stagnating (shocked) plasmas are denoted by indices 1 and 2, respectively.

Equations (4)–(6), in which no magnetic field effect is considered, were well satisfied by the experimental data for these two disparate Z-pinch stagnations (low-power uniform gas puff and high-power discrete wire-array experiments). This analysis concluded that the magnetic field at stagnation, for a wide range of imploding-plasma masses and current amplitudes, in experiments optimizing non-Planckian hard radiation, plays a small role in both the energy and pressure balance, and strongly suggests that only a small fraction of the current flows through the stagnating plasma during the time of radiation emission. A material pressure balance is set between the stagnating and the continuously imploding plasmas, and not by the stagnating-plasma pressure and the magnetic-field pressure (i.e., the Bennett equilibrium). Furthermore, consistently, the total ion kinetic energy in the stagnating plasma was found to be sufficient for providing the energy required for the ionization and radiation from the stagnating plasma. This was also consistent with the fact that the total ion kinetic energy and the pressure in the stagnating plasma were found to be much lower compared to an earlier prediction,^{47,57} which was based on magnetic-field energy dissipation in the stagnating plasma. We note that, consistent with this conclusion, a study by Yu *et al.*⁶⁸ of the three-dimensional effects in the implosion phase showed that the non-uniform nature of Z-pinch implosions is linked to a 3D distribution of trailing mass, which can support current flow at a larger radius, even once the Z-pinch stagnates on axis. While during the period of the hard-radiation emission from the stagnating plasma most of the current continues to flow outside the stagnation region, after the K-emission pulse, additional accelerated plasma and magnetic flux continue to flow inwards.^{44,68}

This work further promoted the need for spectroscopic measurements of the magnetic field radial distribution over the entire imploding plasma volume, and throughout the stagnation process. Such measurements, supporting the conclusions above, will be discussed in Sec. VI C.

B. MHD simulations of the Ne-puff Z-pinch experiments discussed in Sec. II

The extensive data set of K-shell spectroscopy and imaging from the Ne-puff Z-pinch experiment,^{10,11} and the determination of T_i , provided a challenging validation test for Z-pinch simulations. Simulations by Giuliani *et al.*⁶⁹ of this experiment were undertaken to investigate the difference between the ion thermal energy and the ion hydromotion energy revealed in Ref. 11. Calculations were performed using a 2D radiation-magnetohydrodynamic code.⁷⁰ In the simulations, the ion pseudo-temperature T_i^D was calculated using the time dependent, collisional-radiative-equilibrium (CRE) populations of doubly excited states of helium-like neon, then creating synthetic spectra of the Ly- α satellite shape, accounting for Doppler broadening and shift, to determine T_i^D of the ions from the FWHM of the shapes. The results are shown in Fig. 3, and an explanation for the relatively high

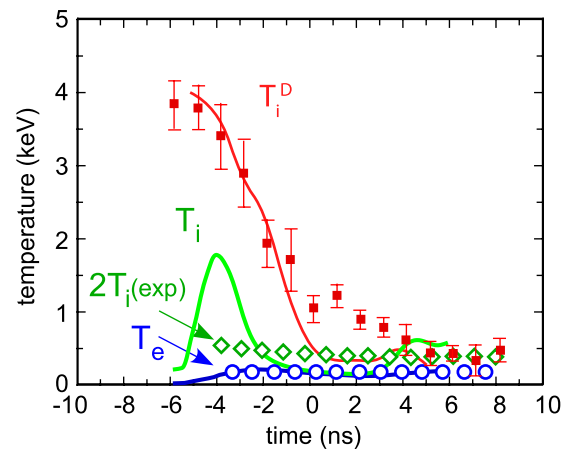


FIG. 3. The measured¹¹ ion Doppler pseudo-temperature shown as solid squares, true ion temperature¹¹ (diamonds), and electron temperature^{10,11} (blue circles). Solid lines represent the calculated ion Doppler pseudo-temperature (red), ion temperature (green), and electron temperature (blue). Reproduced with permission from Giuliani *et al.*, Phys. Plasmas **21**, 031209 (2014).⁶⁹ Copyright 2014 AIP Publishing.

T_i^D early in the stagnation measured in Ref. 11 was explained in Ref. 69 as a combination of compressional ion heating and steep radial velocity gradients near the axis. The calculated electron density in Fig. 6 of Ref. 69 rises rapidly from about -4 ns to the time of the peak K-shell power (0 ns), and is consistent with the range of the measurements, $(6 \pm 3) \times 10^{20} \text{ cm}^{-3}$, limited to times > -2 ns. The rapid rise in the electron density between -4 ns and -2 ns causes a corresponding decrease in the computed ion temperature in Fig. 3 due to thermal equilibration. However, at the early times of stagnations, the computed peak ion temperature of 1.8 keV is much higher than the ion temperature (< 300 eV) found in Ref. 11. This difference seems to indicate that the electron density in the experiment rises earlier and over a longer time span than that found in the computations. It appears that measurements of the electron density prior to -2 ns would be very useful and could reveal additional physics of the stagnation process. Later in the stagnation, the CRE and azimuthal assumptions are less erroneous, making the simulated T_i closer to the true values.

The 3D nature of Z-pinch stagnation was explored using MHD simulation and analytical theory by Yu *et al.*,⁷¹ demonstrating that the non-uniform imploding plasma leads to significant residual kinetic energy at stagnation due to obliquely colliding shocks, local re-expansion of the stagnated plasma, and large-scale vortex formation. However, despite these complicated flows, these simulations confirm the basic pressure balance model described previously, in which the thermal pressure of the stagnated plasma balances the incoming dynamic pressure nmv^2 of the imploding plasma. Hence, even in the fully 3D setting, the 1D shock model described in Sec. III A, based on experimentally determined parameters, was useful in understanding the evolution of spatially averaged quantities.

C. Use of the T_i measurements for an experimental investigation of turbulence in the stagnating Z-pinch plasma

As was discussed in Sec. II, it was shown^{10,11} that the ion temperature at stagnation (a culmination of the plasma implosion) may be an

order of magnitude lower than the pseudo-temperature T_i^D . Thus, the ion kinetic energy at the stagnation phase is dominantly stored in a non-thermal hydrodynamic motion, while at the same time, the plasma appeared by imaging largely uniform at very fine spatial and temporal scales down to about $100\ \mu\text{m}$ and $1\ \text{ns}$, respectively, invoking the question on the nature of this hydrodynamic motion. The studies on the hydromotion at stagnation,^{10,11} and additional studies on the development of turbulence during the implosion⁷² and on the role of the turbulent energy in pressure and energy balance,⁶⁴ stimulated theoretical studies, such as that by Davidovits and Fisch⁷³ on the amplification through compression and viscous dissipation of turbulence during the implosion and stagnation, showing, in particular, how very different plasma turbulence can be from traditional fluid turbulence due to the sensitivity of plasma viscosity to the temperature. Further studies on compressing turbulence in the inviscid, supersonic limit,⁷⁴ then suggested to reconsider, in view of the possible presence of turbulence, two important questions raised by the studies,^{10,11} which are also in the inviscid, supersonic regime: first, what is the nature of this non-thermal hydrodynamic motion, and second, what are its implications in interpreting spectroscopic data (in addition to the obvious Doppler effect).

Supersonic turbulence is a viable candidate for the non-thermal, small-scale motion at stagnation, and thus there should also be self-consistent density fluctuations in proportion to the turbulent kinetic energy. Following a first-principle model for turbulence density distribution,⁷⁵ a new analysis of stagnating pinch data,¹¹ lifting the usual assumption of a uniform plasma, was carried out by Kroupp *et al.*⁷⁶ Since the spectral features (in particular, line intensities) depend on the plasma density non-linearly, certain corrections to the spectroscopically inferred data should be expected. The results of the analysis, shown in Fig. 4(a), indicate a significant correction to the inferred mean plasma density (factor of 2 lower). The emerged picture of supersonically turbulent stagnating plasma appeared not only to be consistent with the observations, but actually improved the agreement with them [Fig. 4(b)].

It should be noted that the mechanism generating the (non-radial) hydrodynamic motion is unclear yet. While energy is deposited in the hydrodynamic motion in the process of stagnation,⁶⁴ this hydrodynamic motion could be seeded by turbulence generated and carried along and even amplified during the compression itself,⁷² or could be generated entirely at stagnation. In either case, there are important implications in various contexts, such as high-current implosions on the Z machine,^{4,12,66,77} a proposed novel fast ignition^{73,78,79} scheme or x-ray burst generation scheme,⁸⁰ and various phenomena of astrophysical interest: molecular cloud dynamics,⁸¹ star formation efficiency,⁸² the core mass/stellar initial mass functions,^{83–85} and Larson's laws.⁸⁶ It may also be relevant in inertial confinement experiments⁸⁷ that observe large quantities of residual hydrodynamic motion. The increase in turbulent energy through compression can be understood by means of a quasi-equation-of-state,^{79,88} although care must be taken in considering whether the compression is in two or three dimensions,⁸⁹ even when the plasma remains inviscid, because the dimensionality of the compression can greatly impact the isotropy of the turbulence. The difference in the behavior of turbulent kinetic energy and thermal energy under compression highlights the importance of further experimental studies of the fundamental phenomenon of turbulence in a compressing plasma.

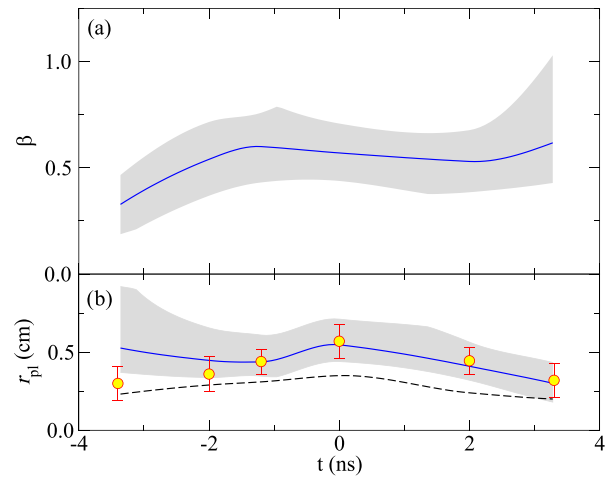


FIG. 4. Results of applying the turbulence density distribution model. (a) The density correction factor β , namely, the ratio between the mean density inferred by accounting for the density fluctuations due to the plasma turbulence and the density inferred assuming uniform density¹¹ (solid line). (b) The plasma column radius r_{pi} : dashed line—uniform-plasma model, solid line—turbulence model. An improved agreement with the experimental data (symbols with error bars) is evident. Reproduced with permission from Phys. Rev. E **97**, 013202 (2018).⁷⁶ Copyright 2018 American Physical Society.

IV. DIRECT DETERMINATION OF THE ION TEMPERATURE IN A HIGH-ENERGY-DENSITY PLASMA USING THE STARK EFFECT

A. The need for developing a direct method for determining the ion temperature in HED plasmas

The studies described in Refs. 10 and 11, bringing up the phenomenon that at a Z-pinch stagnation a significant fraction of the ion kinetic energy can be stored in hydromotion, raised a plausible possibility that similar phenomena also occur in other implosion systems, such as those used for inertial confinement fusion that are pinch-driven⁴ or radiation-driven,^{18,19} or for neutron production.^{16,17,58} Here, we note that even small differences between the pseudo temperature T_i^D and T_i should be investigated since the rates of the fusion processes depend drastically on T_i , while, as also discussed in the context of ICF experiments,⁸⁷ the residual kinetic energy (hydromotion) is irrelevant. Furthermore, in an imploding plasma, as discussed for the Z-pinch stagnation¹¹ and for ICF implosion,⁹⁰ the electron temperature cannot be assumed to represent T_i ; the radial kinetic energy is first transferred to T_i and then to T_e . Thus, the double inequality $T_e < T_i < T_i^D$ holds until the plasma is fully thermalized, which happens at late times, i.e., at times irrelevant for ICF.

It should be noted that in fusion plasmas the ion temperature can also be investigated using spectra of neutrons emitted in various directions. However, this is not straightforward either, since the neutron spectra, similar to the Doppler-broadened line emission, reflect the entire kinetic energy of the ions. Indeed, extensive work has been recently made in both Sandia laboratories⁹¹ and LLNL^{92–94} on the analysis of neutron spectra, in attempts to obtain bounds on the ion temperature and thus to discriminate it from the hydromotion of the fusing particles.

In Refs. 10 and 11 T_i was determined using detailed energy balance for a specific region of the plasma emission that required multiple time- and space-resolved spectroscopic measurements. Such extensive diagnostics and analysis are rarely feasible in more complex HED experiments. This promoted the need to develop a more direct method for determining the ion temperature.

B. Development of the method using the Stark effect

Recently, a more direct measurement of the ion temperature in a HED plasma was developed, only requiring localized instantaneous spectroscopic data.²⁰ The underlying physical phenomenon is the ion-temperature dependence of the Stark profile of certain lines in moderately coupled plasmas.

Stark line broadening is widely used for plasma diagnostics.⁹⁵ The Stark width depends strongly on the plasma density (typically, between $\sim n_e^{2/3}$ and $\sim n_e$), which is true for broadening due to plasma electrons and ions alike. Contrary to that, the temperature dependence is rather weak. However, if n_e and T_e are known with a sufficient precision independently of the line shape measurements (e.g., using the Thomson scattering⁹⁶ or dielectronic satellite ratios⁴⁹), then even the moderate Stark-width sensitivity to T_i can be used to infer the latter.

The Stark effect in a hydrogen-like atom is proportional to the electric field. In an ideal plasma, the electric fields due to the charged plasma particles are distributed according to the Holtmark function,⁹⁷ which is independent of temperature. However, in a non-ideal plasma, characterized by the ion-ion coupling parameter $\Gamma_{ii} = q_i^2/r_i T_i$ (where $r_i = (4\pi n_i/3)^{-1/3}$, and q_i is the ion charge), Coulomb interactions between the particles modify⁹⁸ the Holtmark distribution due to the Debye screening and the repulsion between the ions and the positively charged radiators, resulting in a decrease in the ion-caused Stark broadening. Since the electron broadening is usually smaller than that due to the ions (because of the dynamical nature of the electron perturbation⁹⁵ and the higher ion charge), the total Stark broadening decreases as well. The use of tracer species and transitions for diagnostics should provide sufficient flexibility for employing this approach for determining T_i in a variety of highly non-uniform and transient HED plasmas.

In the specific experiment,²⁰ the x-ray radiation from the stagnation plasma was recorded by a spectroscopic system of three spherical crystals, yielding the shapes of the neon Ly_α satellites, and Ly_δ and Ly_ϵ , as well as providing a 1D imaging of these spectra along the Z-pinch axis. The spectra are recorded at a given instant throughout the stagnation phase using two singly gated intensified charge-coupled device (ICCD) cameras (see Fig. 5). The Ly_α -satellite spectra provided the time-resolved electron density and the total (thermal and hydrodynamic) ion motion at any z position, as was done in Refs. 10 and 11. These parameters were used to infer T_i from the measured Ly_δ and Ly_ϵ spectra (that are affected by the Stark broadening) as outlined below.

Typical spectra at the time of the peak PCD signal ($t = 0$) are shown in Fig. 6. In this example, analyzed are the r -averaged spectra from an axial slice of $\Delta z = 0.5$ mm, centered at $z = 4.5$ mm ($z = 0$ corresponds to the cathode surface). The spectra of Ly_δ and Ly_ϵ were modeled by convolving the calculated Stark lineshapes (using the methods by Stambulchik and Maron^{99,100}) with the Doppler and instrumental broadenings. A best fit is searched for by varying T_i

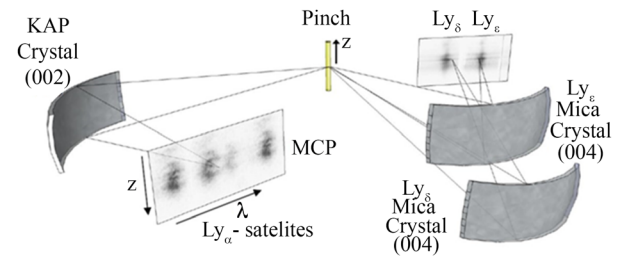


FIG. 5. Schematic of the spectroscopic systems used to measure the spectra of Ly_α -satellites (using KAP second order) and of the high-n-lines (using mica fourth order). The crystals for Ly_δ and Ly_ϵ are placed 20 mm below and above the vertical center of the chamber, respectively, and the crystals are tilted so that the two spectra are recorded on the vertical center of a single MCP. A PCD detector (not shown in the figure) measured the total radiation emitted from $\Delta z = 2$ mm around $z = 5$ mm ($z = 0$ is the cathode surface).

between zero and the pseudo-temperature T_i^D . The results of the high-n line shape analysis are presented in Fig. 7, demonstrating that the best fit is obtained for $T_i = 300$ eV with an estimated uncertainty of ± 150 eV, while assuming $T_i = T_i^D$ results in lineshapes that are wider, far from fitting the data. Such an analysis, repeated for several instants in time, yielded that $T_i \ll T_i^D$ during most of the stagnation, as summarized in Fig. 8. As seen in the figure, T_i and T_i^D as a function of time were found to be similar to those determined by the energy-balance,¹¹ given in Fig. 2.

This direct method for determining T_i is believed to be applicable in various major HED plasma experiments, with some suggestions for implementation details given in Ref. 20.

V. INFERENCE OF THE ION TEMPERATURE AT THE STAGNATION OF A WIRE-ARRAY EXPERIMENT ON THE Z MACHINE

Following the steps in the studies^{10,11} for determining the ion temperature, based on energy balance considerations discussed in Sec. II, an attempt is made here to estimate the ion temperature at the stagnation of a nested-wire-array implosion⁶⁵ on the Z machine.^{4,12,66,77} In this experiment, used were Al wires in the outer array and Ni-cladded Ti wires in the inner array, with the array

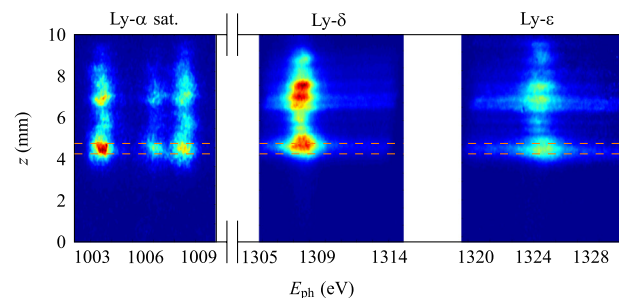


FIG. 6. Ly_α -satellites and high-n-line spectra recorded simultaneously at $t = 0$, axially resolved across the anode-cathode gap. The positions of the hot spots in all three spectra clearly match. The dashed lines highlight the slice for which the data are analyzed. The Ly_α and high-n spectra are normalized to the peak intensities of the Ly_α singlet satellite and Ly_δ , respectively. The anode-cathode gap is 10 mm long ($z = 0$ is the cathode surface). Reproduced with permission from Alumot *et al.*, Phys. Rev. Lett. 122, 095001 (2019).²⁰ Copyright 2019 American Physical Society.

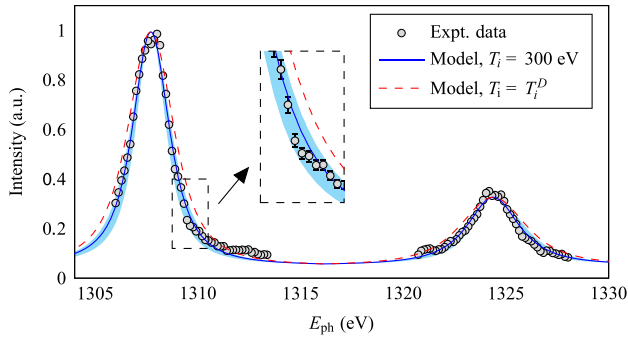


FIG. 7. The experimental high- n spectra are compared to line shape modeling for two values of T_i assumed: 300 eV and T_i^D . $T_i^D = 900$ eV, $N_e = 6 \times 10^{20} \text{ cm}^{-3}$, and $T_e = 200$ eV are assumed for the two cases. The shaded area designates a spread of modeled spectra for T_i varying between 150 eV and 450 eV. An enlarged part of the graph is given in the inset. Reproduced with permission from Alumot *et al.*, Phys. Rev. Lett. **122**, 095001 (2019).²⁰ Copyright 2019 American Physical Society.

diameters being 50 mm and 25 mm, and the wire number in the arrays being 96 and 48, respectively. For this experiment, as described in Ref. 64, a stagnating plasma that is dominated by Ti and Al ions, and is ~ 4 mm in diameter, was diagnosed. Also in this experiment, diagnosed was an on-axis narrower core, 0.9 mm in diameter [as shown in Fig. 9(a); data are taken from Ref. 65] within the Ti–Al core, that was dominated by Ni and Al ions. Time resolved spectroscopic observations, combined with PCD measurements of the radiation emission filtered for various spectral regions, were analyzed by Fisher¹⁰¹ to obtain the electron temperature and density, and the ionic densities for each of the elements in the array, in the narrow (inner) core (similarly to the parameters given for the broader Ti–Al core in Ref. 64). This yielded a total ion density $n_i \sim 5.2 \times 10^{19} \text{ cm}^{-3}$ (i.e., 2.6×10^{19} ,

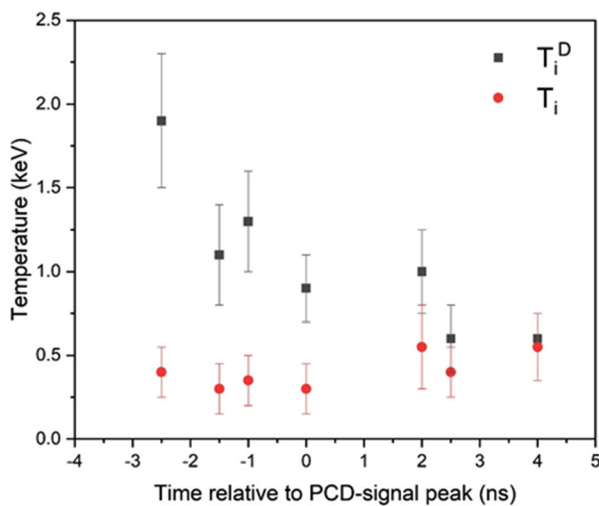


FIG. 8. The measured ion pseudo-temperature T_i^D obtained from the shape of the Ly- α -satellite, and the true ion temperature T_i obtained using the method based on the Stark effect throughout stagnation in a neon-puff Z-pinch experiment (similar to that in Ref. 11). $t = 0$ denotes the time of peak radiation power measured by the PCD.

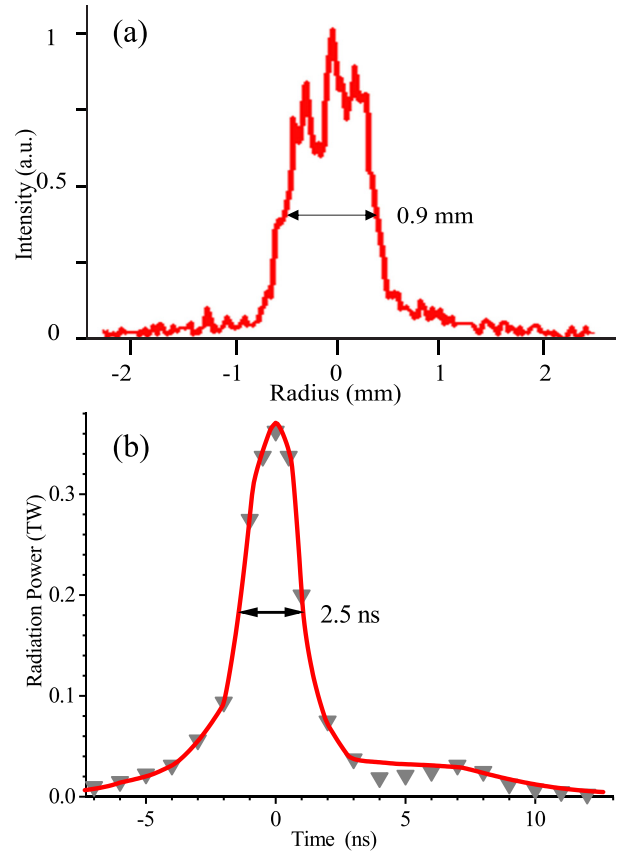


FIG. 9. (a) Radial imaging of Ni He $_{\alpha}$, integrated over the stagnation duration and over the entire pinch length, shows an inner core (found to be dominated by Ni and Al ions—see text) confined to a diameter of 0.9 mm; (b) the data points are obtained from filtered PCD (photo-conducting-device) signals that give the waveform of the total Ni radiation from the inner core, of a FWHM $\tau_{\text{rad}} \sim 2.5$ ns. The curve is a fit to this waveform, obtained by time-dependent atomic-kinetics and radiation-transport modeling¹⁰¹ that determines the electron temperature and composition for this core.

0.47×10^{19} , and $2.1 \times 10^{19} \text{ cm}^{-3}$ for the ionic densities of Ni, Ti, and Al, respectively) and an electron temperature $T_e \sim 2.7$ keV. The average charge state and ion mass in the inner core are ~ 20 and ~ 45 , respectively (larger than in the Ti–Al core described in Ref. 64, due to the larger fraction of Ni in the inner core). Based on these values for the electron temperature and ionic densities in the inner core, the rate τ_{ie} of the ion heat loss to electrons in this core is determined to be ~ 0.8 ns.

The Doppler pseudo-temperature T_i^D of the ions was not measured in this experiment. Thus, we estimate T_i^D in the inner core, averaged over all species in this core, from the total energy radiated during the entire radiation duration and the total number of ions N_{ion} in this core. To this end, we assume that the total energy radiated during stagnation is due to the dissipation of the total ionic kinetic energy $3/2 N_{\text{ion}} T_i^D$ at the stagnating plasma, as substantiated in the experimental studies,^{10,11} and is also consistent with the absence of significant magnetic-field-energy deposition at the stagnating plasma

during the K-radiation emission in this experiment on the Z machine, as discussed in Ref. 64.

In Fig. 9(b) displayed is the filtered Ni ion emission (bound-bound and free-bound) power from the inner core, showing that the emission lasts for $\tau_{\text{rad}} \sim 2.5$ ns. Also shown is a fit to this power based on the time-dependent collisional-radiative and radiation-transport modeling for this core¹⁰¹ mentioned above. This modeling yields that the total energy radiated from the inner core during the entire emission time (2.5 ns) is $Y \approx 5.2$ kJ. N_{ion} is obtained from $n_i V$, where the core volume V is assumed to be that of a cylinder 0.9 mm in diameter and 20 mm in length (which is the entire pinch length in this experiment), i.e., uniformity is assumed here over the pinch column. Using $N_{\text{ion}} = 6.6 \times 10^{17}$ ions obtained gives

$$\overline{T_i^D} = \frac{2}{3} \frac{Y}{N_{\text{ion}}} \approx 33 \text{ keV}. \quad (7)$$

Based on the inferred values given above, we now use [see Eq. (3)]

$$\frac{T_i - T_e}{\tau_{\text{ie}}} \approx \frac{\overline{T_i^D}}{\tau_{\text{rad}}}, \quad (8)$$

to obtain $T_i \approx 13.3$ keV, which is $\approx 0.4 \overline{T_i^D}$.

This estimate is made in the absence of a measurement of $\overline{T_i^D}$, besides being integrated over the duration of the stagnation of the Ni core and over the entire pinch length assuming uniformity. Nevertheless, due to the limited, radially well-defined, region of the Ni core, and the well-defined radiation-emission waveform from this core, one may obtain a plausible range for the true ion temperature. For example, if, due to nonuniformity, the volume of the inner core is only 1/4 of the total nominal volume of the core assumed in the above, the plasma density must be at least $\sqrt{4} \times$ higher in order to provide the total radiation measured (if the plasma is not optically thin a higher density will be required, which will lead to a lower T_i inferred). Therefore, the total number of ions will now be $\approx N_{\text{ion}}/\sqrt{4}$, yielding $\overline{T_i^D} \sim 66$ keV, which gives $T_i \sim 24$ keV, i.e., $\approx 0.4 \overline{T_i^D}$. We note that this value of $\overline{T_i^D}$ (and thus of T_i) is an upper limit, since similarly to the detailed analysis given in Ref. 64 for the broad (Ti–Al) core, based on the assumed implosion velocity of $(7\text{--}8) \times 10^7$ cm/s (not measured for this experiment on the Z-machine) and the account for the energy required for heating and ionizing the plasma in the inner core, one obtains that such a value for $\overline{T_i^D}$ is close to the maximum plausible one (as mentioned above, no additional energy due to magnetic field is deposited at the stagnating plasma during the K-emission duration).

It is interesting to note that in this higher-power experiment on the Z-machine, T_i does not appear to be much lower than $\overline{T_i^D}$, contrary to the low-power experiments discussed in Refs. 11 and 20, where T_i was found to be an order of magnitude lower than $\overline{T_i^D}$. Evidently, this is due to the longer τ_{ie} in the high-power experiment [see Eq. (8)], resulting from the higher electron temperature (2.7 keV vs 0.2 keV), which causes the ions to stay noticeably hotter than the electrons.

VI. DETERMINATION OF MAGNETIC FIELDS IN HIGH-ENERGY-DENSITY PLASMAS

A. Background and early experiments

In general, for pulsed-power systems, knowledge of the magnetic field (B-field) distribution is the only way to obtain the current density

distribution in the various regions of the systems. In addition, it helps to determine the plasma resistivity and the Ohmic-heating distribution, to investigate the plasma dynamics (through the $\mathbf{J} \times \mathbf{B}$ forces) and energy balance, and to infer the particle magnetization.

The two most common non-intrusive methods for the B-field determination in such plasmas are based on the splitting of emission or absorption lines in the plasma due to the Zeeman effect, or on the change of an external light-beam polarization due to the Faraday-rotation effect. Each of these two common methods has its challenges and limitations. In particular, the plasma conditions that are typical of high-energy-density (HED) systems often render the Zeeman-splitting magnetic-field diagnostics impossible. The high densities and high ion velocities result in broad spectral line-shapes that smear out the Zeeman-split patterns, even when polarization techniques are employed for the suppression of the π components of the spectrum. For the Faraday-rotation method, the rotation of the plane of polarization of an electromagnetic wave passing through a plasma is proportional to $\int n_e \mathbf{B} \cdot d\mathbf{l}$, where n_e is the electron density and l is the coordinate along the line of sight (e.g., Refs. 102 and 103). Therefore, Faraday rotation requires knowledge of the electron density at all locations in which the light polarization is affected, and is also an integrated measurement over the line of view, along which usually both B and n_e vary, which is likely to lead to ambiguous interpretation of the data. Moreover, in chordal measurements in imploding plasmas reconstructing the magnetic-field radial distribution requires assuming a cylindrical symmetry, which is usually unpredictable and far from reality, and thus may lead to very large errors, see, for example, discussion in Ref. 104. An alternative approach is based on proton beam deflectometry (e.g., Refs. 105–109) that requires means for proton beam generation and integration of the effects of B and the electric field E on the proton trajectory over the entire proton path. For these reasons, extending the usefulness of the methods based on the Zeeman effect to HED conditions is highly desirable.

An early spectroscopic measurement of the magnetic field in a pulsed-power system was performed in a planar ion diode.¹¹⁰ In this work, transitions of a dopant element on the anode surface were used to yield the time-dependent magnetic field on the anode surface with an accuracy of $\pm 6\%$, as shown in Fig. 10. The plasma density was low enough, $\sim 10^{15}$ cm⁻³, allowing for the Zeeman splitting to be observed. These measurements allowed for determining the diamagnetic effects of the Brillouin electron flow in the diode acceleration gap,¹¹¹ which also helped to determine the resistivity of the anode plasma penetrated by the diamagnetic component, and also showed a significant electron flow beyond the calculated¹¹¹ electron-sheath region. The latter finding was consistent with electric-field measurements in the diode gap of a similar diode^{112,113} that showed a drift of the electron cloud much closer to the anode than predicted, and with electric-field measurements in the diode gap of the Particle Beam Fusion Accelerator II (PBFA-II) ion diode at Sandia^{66,114–116} that demonstrated similar findings. Other early efforts to spectroscopically measure magnetic fields in pulsed-power systems can be found in Refs. 117 and 118.

As said above, for higher plasma densities in pulsed-power systems, smearing of the Zeeman splitting is likely. In Fig. 11, we demonstrate the limitation of the Zeeman-split diagnostics due to the Stark broadening. The figure shows the Zeeman pattern in the Al III 4s–4p doublet transition for $B = 4$ T, assuming Doppler broadening due to $T_i = 5$ eV, together with a convolution of this pattern with a 3-Å

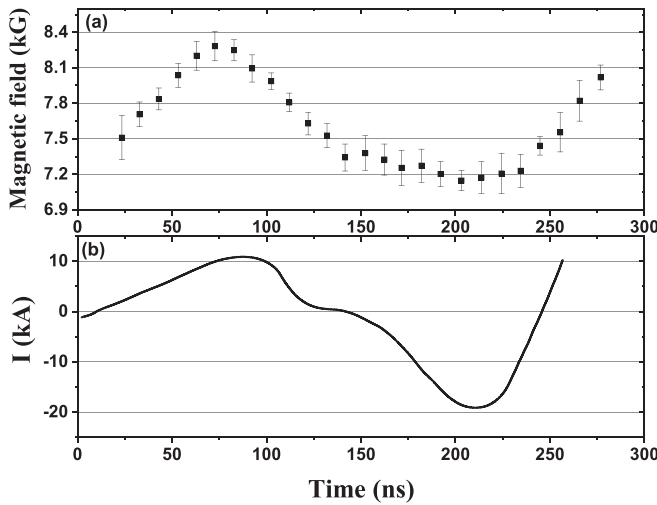


FIG. 10. (a) Magnetic field as a function of time at the plane of the anode surface in a magnetically insulated ion diode. Used is a Zeeman splitting of the Ba II 6142-Å emission line, with Ba introduced as a dopant on the anode surface. The initially applied (insulating) magnetic field (parallel to the anode) is 7.6 kG. The electron Brillouin flow in the diode due to the current pulse of ≈ 100 ns duration causes a rise in B on the anode side that penetrates the plasma, and is observed by the dopant emission. (b) Total diode current waveform. Reproduced with permission from Maron *et al.*, Phys. Rev. A **39**, 5856 (1989).¹¹⁰ Copyright 1989 American Physical Society.

Lorentzian that corresponds to a Stark broadening for $n_e \sim 5 \times 10^{17} \text{ cm}^{-3}$; the latter completely smears out the splitting. Similar difficulty may arise due to a large Doppler broadening. Therefore, progress in the B-field measurements in imploding plasmas requires extending the spectroscopic diagnostics to conditions in which the Zeeman-split pattern is not resolvable. A discussion on the application regimes and limitations of the methods that extend the Zeeman-based spectroscopy is given by Doron *et al.*¹¹⁹ Here, we describe the progress

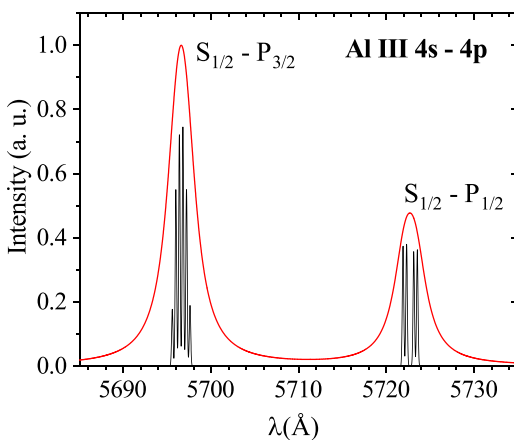


FIG. 11. Zeeman effect of the Al III 4s–4p doublet, calculated for a magnetic field of 4 T and convolved with Voigt profile due to a 0.2-Å FWHM Doppler-Gaussian ($T_i = 5$ eV) and a 3-Å Lorentzian ($n_e = 5 \times 10^{17} \text{ cm}^{-3}$). Also shown is the Zeeman pattern without the Lorentzian broadening.

in the B-field measurements using these methods and the impact of the findings on the understanding of pulsed-power systems.

B. Measurements of magnetic field in Z-pinch

The first measurement, to the best of our knowledge, of the B-field in Z-pinch experiments was made by Davara *et al.*¹²⁰ In this work, the radial distribution of the azimuthal B-field was measured as a function of time during the implosion of a CO₂ puff driven by a ~ 300 kA, 1.6- μs current pulse. The measurements utilized the polarization properties of line emission observed perpendicular to the magnetic-field direction. The principle of the technique is shown in Fig. 12. The field is determined by detecting the relative contributions to the line shape of the π and σ Zeeman components that, since observed perpendicular to B, are of orthogonal linear polarizations. Shown in the figure is the simulation of the Al III 4s–4p doublet spectrum for $B = 5$ T and $n_e = 10^{18} \text{ cm}^{-3}$, together with the shapes of the π and σ polarizations. It can be seen from the figure that the orthogonally polarized spectral lines have different linewidths. Since this difference is proportional to the B-field magnitude, it can be used for the field diagnostics.

In this study, end-on observations of the plasma shell were used, as shown in Fig. 13. In general, since the linewidth difference is rather small, a reliable measurement requires a high signal/noise ratio; thus, an averaging of the measurements for each polarization over many discharges was required. An example of the measured line profiles recorded in the different π and σ polarizations, demonstrating the width difference that is used for the B-field determination, is given in Fig. 14.

The time-resolved radial distributions of the magnetic field shown in Fig. 15¹²⁰ demonstrate the rise of B due to the compression and due to the rise of the circuit current. For explaining the distribution of B in the shell, we solved the diffusion equation of B,

$$\frac{\partial B_\theta}{\partial t} = \frac{1}{\mu_0 \sigma} \frac{\partial^2 B_\theta}{\partial \xi^2}, \tag{9}$$

where a planar geometry was assumed (justified by the large radius relative to the radial width of the zone addressed), $\xi = R_0(t) - r$ is the distance between the plasma outer radius $R_0(t)$ and any point in the

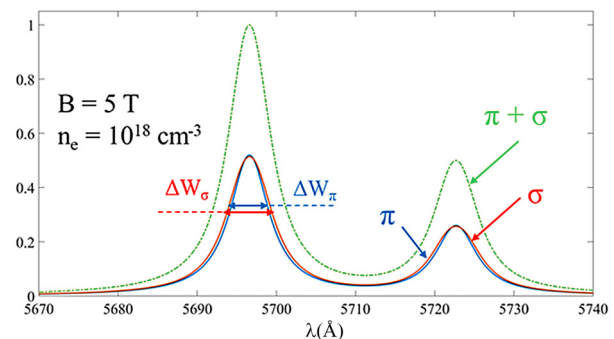


FIG. 12. Simulation of the Al III 4s–4p doublet for $B = 5$ T and $n_e = 10^{18} \text{ cm}^{-3}$, assuming line-of-sight perpendicular to B: total emission (green), π (blue), and σ (red) linear polarizations.

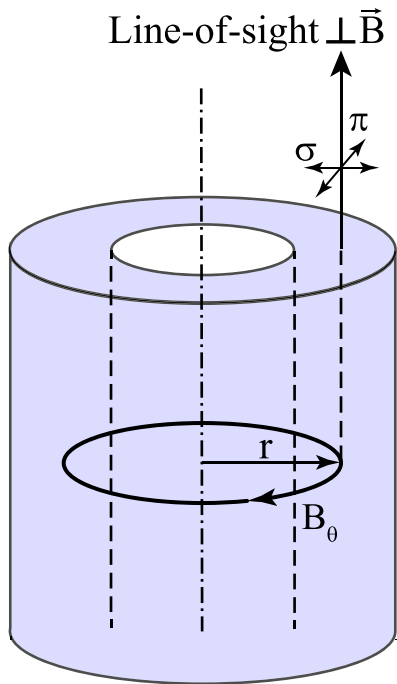


FIG. 13. A schematic description of the end-on observation of the Z-pinch, providing a line-of-sight perpendicular to the compressing azimuthal magnetic field, giving the Zeeman π and σ orthogonal linearly polarized emissions.

plasma, and σ is the plasma conductivity. Used are the boundary conditions

$$B_{\theta}(\xi, t = 0) = 0, \quad B_{\theta}(\xi = 0, t) = B_0(t), \quad (10)$$

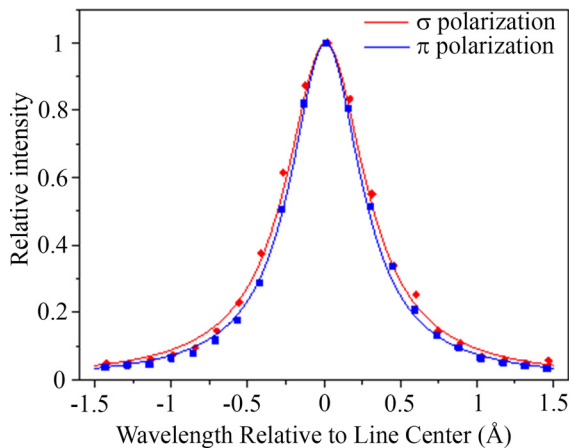


FIG. 14. Example of the measured profiles for the π and σ polarizations of the O IV 3063.5 Å line for $t = 480$ ns after the current discharge, each obtained by averaging over 20 discharges. The uncertainties are given by the size of the data points. The FWHM of the Lorentzian fits are 0.56 ± 0.01 Å (π) and 0.62 ± 0.01 Å (σ), giving $B = 1.8 \pm 0.3$ T. The uncertainty in the FWHM is determined from the difference between the widths of profiles fitted to the upper or lower bounds of the data points. Reproduced with the permission from Davara *et al.*, Phys. Plasmas **5**, 1068 (1998).¹²⁰ Copyright 1998 AIP Publishing.

where $B_0(t)$ is the B-field at the radial outer-boundary of the plasma. The solution of Eq. (9) is¹²¹

$$B(\xi, t) = \sqrt{\frac{\mu_0 \sigma}{4\pi}} \int_0^t \frac{B_0(\tau)}{(t - \tau)^{3/2}} \times \sum_{n=-\infty}^{+\infty} \left\{ (\xi + 2nl) \exp \left[-\frac{\mu_0 \sigma (\xi + 2nl)^2}{4(t - \tau)} \right] \right\} d\tau, \quad (11)$$

where l is the thickness of the plasma shell ($\xi < l$) and t is the time of the observation. Here, l is assumed to be constant since the solution is insensitive to l for $l \geq 0.5$ mm, while l was measured to be ≈ 0.7 mm for the entire period over which the magnetic field was measured. By fitting the solution to the measured time-dependent radial distributions of B , the conductivity of the plasma was determined and found to be nearly in agreement with the Spitzer value. The latter is estimated from the electron density and temperature determined from spectroscopic observations for the same plasma^{120,122–124} giving $\sigma \approx 2 \times 10^4 \Omega^{-1} \text{ m}^{-1}$ at the outer edge of the plasma ($T_e = 13$ eV and $\bar{Z} = 3.8$), and σ in the inner edge is $\approx 10^4 \Omega^{-1} \text{ m}^{-1}$ ($T_e = 5$ eV and $\bar{Z} = 2$).

In writing the diffusion equation [Eq. (9)], we assumed a uniform conductivity; the average conductivity across the current layer. When the conductivity is nonuniform, a nonlinear advection term, $-\frac{1}{\mu_0} \frac{\partial(1/\sigma)}{\partial \xi} \frac{\partial B_{\theta}}{\partial \xi}$, has to be added on the left-hand side of the equation. It was shown by Gourdain *et al.*¹²⁵ that, due to large resistivity gradients, the nonlinear advection term can significantly affect the penetration of the magnetic field. However, in Ref. 125 the scale length of the conductivity variation was much smaller than the current layer width, while in the experiment described here, the scale length of conductivity variation is larger than the current layer width. As said above, the conductivity at the outer edge is higher by less than 50% than that in the inner edge of the current layer; therefore, the effect of conductivity gradients is small.

The magnetic-field distribution measured, together with the electron temperature and density distributions determined^{122,123} for the

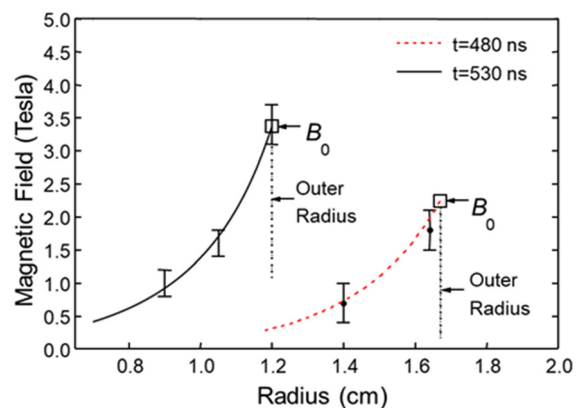


FIG. 15. The magnetic-field distribution in the imploding plasma at different times. The fitting curves are based on the solution of a 1D magnetic-field diffusion equation for each time using a plasma conductivity that is constant over the plasma shell, where $\sigma = 3.1 \times 10^4 \Omega^{-1} \text{ m}^{-1}$ and $2.7 \times 10^4 \Omega^{-1} \text{ m}^{-1}$ for $t = 480$ ns and 530 ns, respectively. The time of stagnation is ≈ 620 ns (see text). B_0 is the field magnitude at the outer edge of the plasma; Reproduced with the permission from Davara *et al.*, Phys. Plasmas **5**, 1068 (1998).¹²⁰ Copyright 1998 AIP Publishing.

same plasma, were used to study the history of the magnetic-field energy coupling to the plasma by comparing the energy deposition and dissipation rates in the plasma, and by assessing the pressure terms, as a function of radius and time.¹²³ This analysis allowed for concluding that $\sim 2/3$ of the energy deposited in the plasma up to the last stage of the implosion is imparted onto the plasma radial flow, while the rest of the energy is converted into internal energy and radiation. In addition, the measured magnetic-field distribution allowed for determining the energy terms in the implosion phase, which helped explaining the propagation of an ionization wave in the imploding plasma¹²⁴ and, thus, the time-dependent radial distribution of the ionic charge states in the plasma.¹²⁶

It should be emphasized that in this work the radial B-distribution could only be measured for radii > 8 mm and up to ~ 90 ns prior to stagnation. At smaller radii or at times closer to stagnation, the Stark and Doppler broadenings were too dominant to allow for determination of the linewidth difference of the two polarizations.

We mention here that polarization spectroscopy was used to determine B in the outer regions of a gas-puff implosion by Golingo *et al.*¹²⁷ Also, observation of the Zeeman splitting was used by Gomez *et al.*¹²⁸ to determine B in the outside region of an imploding liner in a ~ 20 MA experiment on the Z machine.

C. Measurements of B-field distribution throughout stagnation

Improving our understanding of the stagnation process and validation of simulation codes require measuring B throughout the plasma shell and throughout stagnation. As discussed in Sec. III, spectroscopic data strongly suggested⁶⁴ that only a small fraction of the drive current was flowing through the stagnating plasma, which stimulated direct measurements based on the Zeeman effect.

Such measurements were recently performed by Rosenzweig *et al.*,^{129,130} where determined was the B-field radial distribution in the shell throughout stagnation. In this work, chordal lines of sight were used to observe the Zeeman effect as a function of radius. A formidable difficulty in measuring B as a function of radius over the entire imploding plasma is due to the integration of the spectra along the line of sight. Generally, this means that Abel inversion of the data is required, which in imploding plasma experiments, is likely to lead to misleading results due to the common azimuthal nonuniformity of the plasma and the low signal-to-noise ratio in the data. Thus, it is essential to find ways to perform local measurements in radius, i.e., avoiding the need for Abel inversion. In addition, due to the common irreproducibility in pulsed-power experiments, determining B in various radii simultaneously in a single discharge is desirable. In the work, described in Refs. 129 and 130, both challenges were addressed. This was achieved by taking advantage of the naturally formed gradients in the plasma conditions that lead to variation of the ionic charge state with radius, as in Foord *et al.*¹²⁶ Measuring the field by utilizing an emission line of a certain charge state, while looking chordally at the outermost region in which the charge state is present, ensures a line of view parallel to the field and at a region limited in the radial and azimuthal dimensions, i.e., yielding B at the radius of this region (see Fig. 16). Moreover, since line shapes of transitions of different charge states can be recorded simultaneously, observing lines from several charge states (each by looking at the outer region of the respective emission)

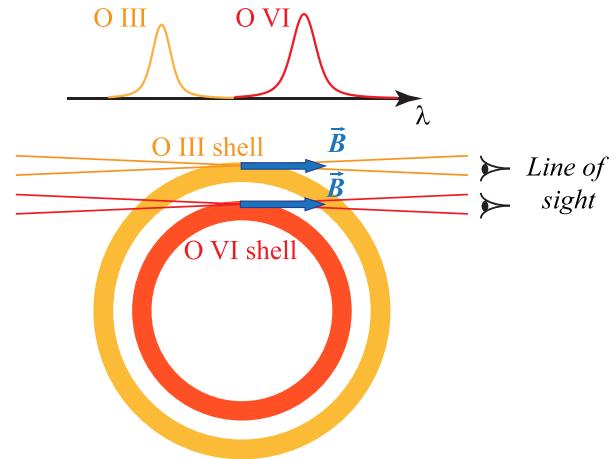


FIG. 16. Schematic of measurements of the B-field radial distribution by utilizing the emission lines of different charge states that are abundant within different radii. Observing the line emission from the outermost radius in which each charge-state emits provides radially resolved data without the need for an Abel inversion. It also ensures viewing parallel to \mathbf{B} , which is crucial for polarization spectroscopy used in this experiment.

provides the magnetic field magnitude at several radii, yielding the field radial distribution in a single experiment.

In these measurements, since the line of sight is parallel to B, utilized for the determination of B is the spectral separation between the $\sigma+$ and $\sigma-$ components of the Zeeman emissions pattern. The wavelength separation between these two components is then used for the field determination, as demonstrated in Fig. 17 and described in several Refs. 117, 127, and 131–133. When applicable, this method is the most sensitive (among the Zeeman-effect-based methods) to the magnetic field.¹¹⁹ In addition, this method is nearly unaffected by opacity since it relies on the line positions rather than on their shapes.

An example of the measured B-field distribution is presented in Fig. 18. Using

$$B = \frac{\mu_0 I}{2\pi R}, \tag{12}$$

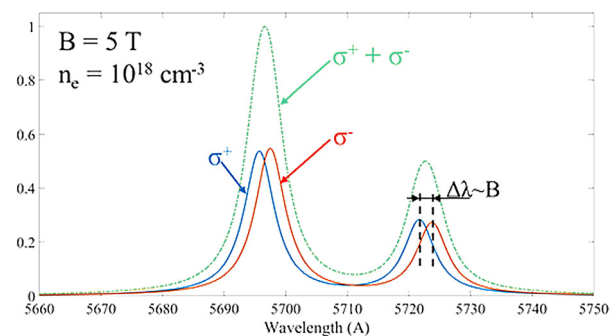


FIG. 17. Simulation of the Al III 4s–4p doublet at $B = 5$ T and $n_e = 10^{18} \text{ cm}^{-3}$, assuming a line of sight parallel to \mathbf{B} : total emission (green), and σ^+ (blue) and σ^- (red) circular polarizations.

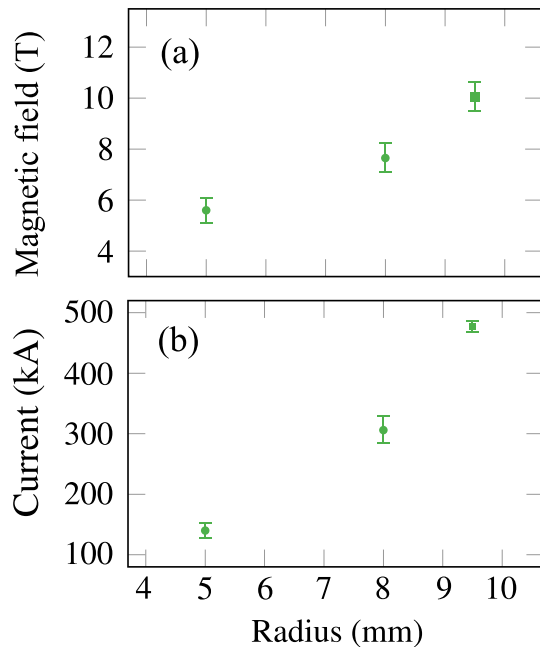


FIG. 18. Magnetic field distribution (a) and integrated current distribution (b) at $t = -15.5$ ns (where $t = 0$ refers to the radiation peak time) in the middle of the 9-mm-long A-K gap. The circles represent values obtained from O VI ($R \approx 5$ mm) and O III ($R \approx 8$ mm) spectral lines, and the squares represent the magnetic field B_0 at the outer radius R_0 of the plasma, obtained from the total current. Reproduced with the permission from Rosenzweig *et al.*, *Phys. Plasmas* **27**, 022705 (2020).¹³⁰ Copyright 2020 AIP Publishing.

where B is the field value measured at the radius R and I is the axial current within a cylinder of this radius, each such data point yields, to a good approximation, the total current flowing within the respective radius, producing a current profile from which the current density can be derived.

The radial distribution of the B-field throughout stagnation at several axial locations, including close to the axis,^{129,130} demonstrated several striking features. Most remarkably, the peak field remains at a radius much larger than the stagnation radius at all times. The current flowing through the stagnating plasma is found to be only a small fraction of the total current. This constitutes the first direct confirmation of the conclusion, originally based on the pressure and energy balance considerations,⁶⁴ that the magnetic field pressure and energy play an insignificant role at the plasma stagnation.

Also in this work, the B-field data taken over several axial positions are used to obtain the true inductance in the imploding plasma,¹³⁰ demonstrating that imaging data or electrical measurements are insufficient for this purpose.

A surprising observation in these measurements is that while the distribution observed is sometimes monotonic with respect to the radius, more often it is not—a behavior that can be linked to 2D features in the plasma column resulting from the Rayleigh–Taylor instability. Such distributions were not seen in the simulation of this experiment, which at all times produced a magnetic field that rises from $r = 0$ to the vacuum-plasma boundary R_0 , and then drops as $1/r$ according to Eq. (12). To understand this finding, visible-UV

imaging was performed showing an onset of the Rayleigh–Taylor instability that grows as the implosion progresses. At the final stages of the implosion, the instability grows to form flaring arcs that curve toward the anode. A similar behavior, even more pronounced, was recorded for neon gas-puff implosions in the same generator by Osin *et al.*,¹³⁴ and further discussed by Giuliani *et al.*⁶⁹ To further probe into these findings, we now obtain the induction equation by beginning with Faraday’s law

$$\frac{\partial \vec{B}}{\partial t} = -\nabla \times \vec{E}, \quad (13)$$

and combining it with Ohm’s law, neglecting the pressure term for the axial electric field in the plasma,

$$E_z = -v_r B_\theta + \eta J_z = -v_r B_\theta + \frac{\eta}{\mu_0} \frac{1}{r} \frac{\partial}{\partial r} (r B_\theta), \quad (14)$$

yields

$$\frac{\partial B_\theta}{\partial t} = \frac{\partial}{\partial r} (v_r B_\theta) - \frac{\partial}{\partial r} \left(\frac{\eta}{\mu_0} \frac{1}{r} \frac{\partial}{\partial r} (r B_\theta) \right), \quad (15)$$

where η is the plasma resistivity and v is the radial velocity. Using the properties determined for the plasma, namely, $T_e \approx 7$ eV, $n_e \approx 1.5 \times 10^{18}$ cm⁻³, $B = B_\theta \approx 10$ T, $Z \approx 2$, $R_0 \approx 8$ mm, and $\eta = \eta_{\text{Spitzer}} \approx 2.5 \times 10^{-5}$ Ω m,¹³⁰ it is shown that Eq. (15) is dominated by the first term, i.e., the plasma is dominated by advection (the magnetic field is partially “frozen in” the plasma). Thus, plausibly, the axial plasma flow that accompanies the flaring arcs formation carries the partially frozen-in magnetic field and distorts the 2D contours of its $r - z$ distribution. This distribution can result in a non-monotonic radial distribution when viewed within a narrow Δz window provided by the diagnostic system, if the flaring arc crosses the measured z -position. This was supported by the 2D images that showed that a non-monotonic distribution for the magnetic field at a particular z position is always associated with a flaring arc at the same z position.¹³⁰ Further computational discussion will be given separately.¹³⁵

D. Measurements of B having an arbitrary direction

While the two polarization-based methods described above have proven to be useful for advancing our understanding of Z-pinch physics, they both require that the B-field has a dominant direction. However, when the magnetic-field direction varies in time or over spatial scales that are below the diagnostic system resolution, polarization techniques are either inapplicable or provide ambiguous results. In such cases of “non-directional” fields, the only known available spectroscopic approach is that developed by Stambulchik *et al.*,¹³⁶ which is based on the comparison of line shapes of different fine-structure components of the same multiplet.

The principle of this method is illustrated in Fig. 19. It is based on the fact that the different fine-structure components of the same atomic multiplet undergo different Zeeman splittings, while the other line-broadening mechanisms, namely the Stark and the Doppler effects, and the instrumental broadening, are practically identical for the two components. Generally, $^2S-^2P$ type transitions are favorable candidates for this diagnostics since the relative linewidth difference between the doublet components ($^2S_{1/2}-^2P_{1/2}$ and $^2S_{1/2}-^2P_{3/2}$) is most sensitive to the magnetic field; the $1/2-1/2$ component being wider.

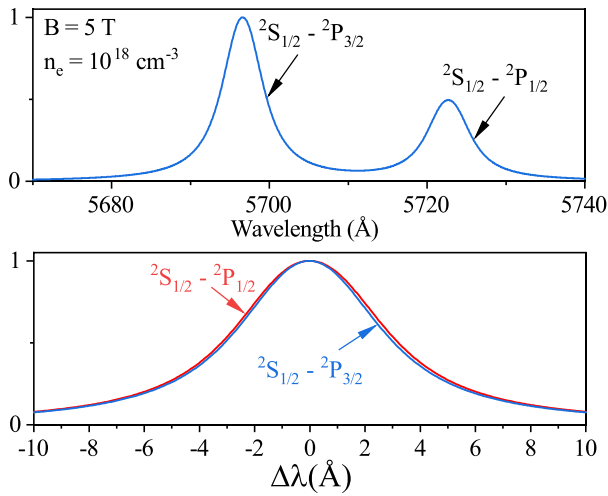


FIG. 19. Upper panel: simulation of the Al III 4s–4p doublet for $n_e = 10^{18} \text{ cm}^{-3}$ and $B = 5 \text{ T}$. Lower panel: the comparison between the peak-normalized line shapes of the two doublet components shows a difference in the linewidths, revealing the presence of the magnetic field.

Therefore, if these two multiplet components are recorded simultaneously, the difference between the line shapes, that is only due to the magnetic field, can be used for the field determination. Since the diagnostics does not rely on the emission polarization properties, it is applicable to non-directional magnetic fields. Also, since the opacity effect (if present) acts in the opposite directions, i.e., the broadening caused by self-absorption is more pronounced for the stronger and narrower component (${}^2S_{1/2} - {}^2P_{3/2}$), then even if the plasma opacity is not accounted for accurately, the measurements still yield a lower limit of the magnetic field.

In the high-density conditions of HED plasmas, the two fine-structure components may significantly overlap. In such a case, a simple comparison of the multiplet line shapes for inferring the field, as shown in Fig. 19, is inadequate. Nevertheless, the diagnostics is still useful if detailed line shape simulations⁹⁹ of the entire multiplet are made, also yielding information on n_e . Obtaining a good fit to the experimental data using many time-consuming runs of detailed line shape calculations for different combinations of the fitting parameters (B , T , n_e), might be not practical. Instead, if the Stark and Zeeman effects can be assumed to be independent, the total line profile can be expressed as a convolution of the two profiles, i.e.,

$$I(B, T, n_e; \omega) = \int d\omega' I_Z(B, \omega') I_S(T, n_e, \omega - \omega'), \quad (16)$$

where the (static) Zeeman pattern $I_Z(B; \omega')$ is calculated using a fast code¹³⁷ and the Stark profile $I_S(T, n_e; \omega)$ is assumed to be a shifted Lorentzian (i.e., an isolated-line shape calculated in the impact approximation⁹⁵)

$$I_S(T, n_e; \omega) = \frac{1}{\pi} \frac{w(T, n_e)}{[\omega - \omega_0 - d(T, n_e)]^2 + w^2(T, n_e)}. \quad (17)$$

Here, $w(T, n_e)$ and $d(T, n_e)$ are, respectively, the Stark half-width at half-maximum (HWHM) and the Stark shift parameters value, and ω_0 is the unperturbed line position.

This approach was demonstrated^{136,138} for measuring B and n_e in a laser-produced plasma plume under an externally applied magnetic field.

E. B-field measurements in high-current self-focusing electron diode

In high-current electron diodes, the self-generated magnetic field causes electron-beam focusing at the center of the anode, as discussed by Hahn *et al.*¹³⁹ and Johnston *et al.*¹⁴⁰ Generally, plasma is formed all over the anode surface during and after the process of the beam focusing.¹⁴¹ Knowledge of the beam current profile, which can be obtained from the B-field distribution, is required for understanding the pinch dynamics and for optimizing the diode performance. The magnetic field was determined in the anode plasma in the Sandia 10-MV, 200-kA electron beam diode by Patel *et al.*,¹⁴² where the Zeeman effect in transitions of carbon ions present in the anode plasma was recorded, yielding the B-field in various radial positions near the anode surface.

Also for this diode, the radial distribution of B in the anode plasma for different distances from the anode surface was inferred by Biswas *et al.*,¹⁴³ using the data obtained by Johnston *et al.*¹⁴⁰ Figure 20 presents an example of the experimental data of the C IV ${}^2S_{1/2} - {}^2P_{1/2}$ component, recorded for different distances from the diode axis at 0.75 mm away from the anode surface. The fits of the line shape computations (also shown in Fig. 20) to the data yield both the B-field and the electron density from the Stark broadening.

In this work, the measured B-field as a function of distance from the anode surface allowed for determining quantitatively the shielding of the magnetic field in the anode plasma. It also allowed for fitting the variation of B with the distance from the anode surface (namely, from the vacuum gap across the plasma to the anode surface), to a solution of the diffusion equation, which yielded the plasma resistivity. The latter was found to be close to the Spitzer resistivity value for this plasma,

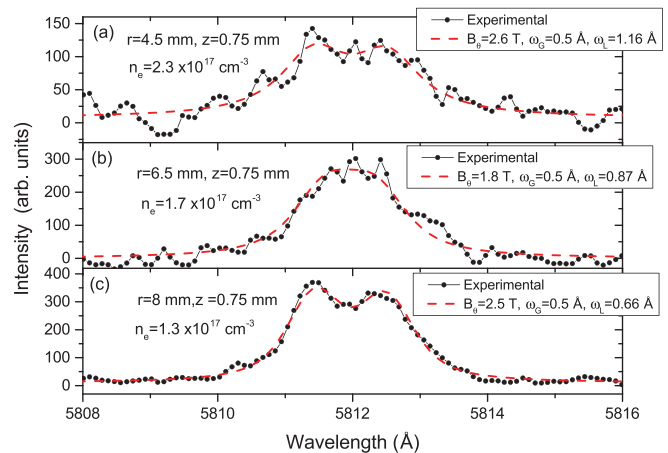


FIG. 20. C IV 3s–3p ${}^2S_{1/2} - {}^2P_{1/2}$ component from the region 0.5–1 mm from the anode surface, at different radii, after Inverse-Abel transformation. Dashed (red) curves are the simulated spectra obtained by convolving the Zeeman profile with the Stark and instrumental profiles. In the legend, B_θ , ω_S , and ω_I are the azimuthal magnetic field, the Stark FWHM, and the instrumental FWHM used for the fit, respectively. Reproduced with the permission from Biswas *et al.*, *Phys. Plasmas* **25**, 113102 (2018).¹⁴³ Copyright 2018 AIP Publishing.

estimated using the electron temperature and charge-state distribution determined from line-intensity ratios.¹⁴³

VII. MAGNETIZED PLASMA COMPRESSION

Magnetized plasma compression (MPC) refers to a configuration of a Z-pinch with a pre-embedded axial magnetic field. In these experiments, the plasma and the embedded field are compressed by the azimuthal magnetic field due to the axial current driven in the plasma. The main goal of the first experimental MPC studies^{144,145} was the generation of ultra-high magnetic fields. Indeed, a 420-fold compression of B-field to a magnitude of 4200 T was demonstrated.¹⁴⁴ In addition, a few studies^{146–150} discussed the stabilization effect of the pre-embedded B_z on the plasma implosion. In the last decade, the interest in MPC has dramatically grown due to the path to fusion introduced at Sandia National Laboratories, based on the compression of initially heated magnetized plasma.^{3,6} The large pre-embedded magnetic field used in these experiments helps to inhibit the radial thermal conduction, and, at stagnation, to trap the high-energy fusion products. Since then, MPC is studied in most major Z-pinch laboratories.

A fundamental study of MCP was made by Mikitchuk *et al.*,¹³³ revealing an unpredicted phenomenon, where even a weak initially applied axial magnetic field has a significant impact on the current distribution in the plasma: during the implosion, a large part of the current is diverted from the imploding plasma to a low-density plasma residing at large radii. These results were achieved by pioneering spectroscopic measurements of both the azimuthal (compressing) and axial magnetic fields, as a function of space and time throughout the implosion.^{133,151} Systematic magnetic-field measurements were made utilizing the polarization-based spectroscopic technique for light emission viewed parallel to the magnetic field, as discussed in Sec. VI C. The results are summarized in Fig. 21, where shown are the measured B_θ at the plasma outer radius, for different initial axial magnetic fields (B_{z0}), together with B_θ expected, calculated by assuming the entire circuit current flows within the plasma outer radius [see Eq. (12), where here the outer radius is defined at 20% of the peak emission intensity radial distribution obtained by the inverse Abel transform]. For B_{z0} = 0, the measured B_θ shows that the entire current flows within the imploding shell. However, for B_{z0} > 0, the measured B_θ is significantly lower than expected. This shows that the application of B_z significantly affects the current distribution in the plasma, such that only a small part of the current flows through the imploding plasma. Furthermore, it is seen that the fraction of the total current that flows in the imploding plasma decreases with B_{z0}.

To explain this phenomenon, a model for the current distribution evolution that is based on the development of a force-free current flow^{133,152} in the peripheral, low-density plasma was suggested. In this model, a plasma in a uniform and constant electric field $\vec{E} = (0, 0, E_z)$ and magnetic field $\vec{B} = (0, B_y, B_z)$ is considered. The evolution of the plasma velocity (\vec{v}) and current density (\vec{j}) in the low-density plasma is obtained by solving the coupled equation of motion and generalized Ohm's law,

$$\rho \frac{d\vec{v}}{dt} = \vec{j} \times \vec{B}, \tag{18}$$

$$\frac{d\vec{j}}{dt} = \frac{\nu_{ei}}{\eta} (\vec{E} + \vec{v} \times \vec{B}) - \nu_{ei} \vec{j} - \omega_{ce} \frac{\vec{j} \times \vec{B}}{|\vec{B}|}, \tag{19}$$

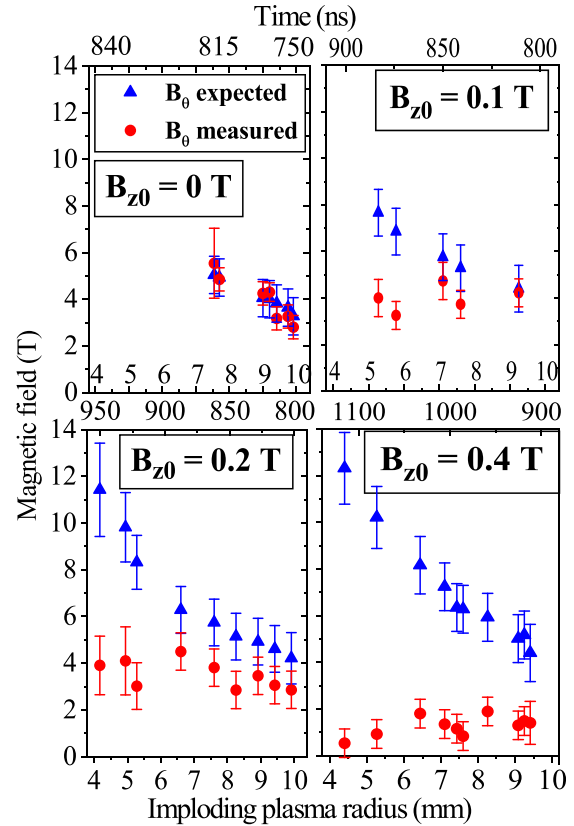


FIG. 21. B_θ as a function of the outer imploding-plasma radius, measured for B_{z0} = 0, 0.1, 0.2, and 0.4 T, together with the expected B_θ, calculated using the total current. The upper scale shows the typical times that correspond to each plasma radius (times of stagnation for B_{z0} = 0, 0.1, 0.2, and 0.4 T are 860 ± 20, 920 ± 20, 1030 ± 30, and 1160 ± 40 ns, respectively). Reproduced with permission from Mikitchuk *et al.*, Phys. Rev. Lett. **122**, 045001 (2019).¹³³ Copyright 2019 American Physical Society.

where ρ is the plasma mass density, ν_{ei} is the electron-ion collision frequency, η is the plasma resistivity, and ω_{ce} is the electron cyclotron frequency. These equations can be solved analytically¹⁵¹ and their asymptotic solution gives the force-free current configuration and the $E \times B$ drift plasma velocity

$$j_z = \frac{E_z}{\eta} \frac{B_z^2}{B_z^2 + B_y^2}, \tag{20}$$

$$j_y = \frac{E_z}{\eta} \frac{B_z \cdot B_y}{B_z^2 + B_y^2}, \tag{21}$$

$$\vec{v} = \frac{E_z B_y}{B_z^2 + B_y^2} \hat{x}. \tag{22}$$

The solution also provides the characteristic timescale for the establishment of the force-free configuration

$$\tau_{steady} = \frac{\nu_{ei}}{\omega_{ce} \omega_{ci}}. \tag{23}$$

We point out that this model does not include Maxwell equations, which are required in order to obtain a more realistic evolution

of the plasma and the current. Modeling that involves processes beyond MHD is required to explain the observed phenomena and to test our hypothesis. Simulations of this kind have been recently published.^{153,154} However, the present simplified treatment presents the possible governing process of the current evolution in this MPC experiment.^{133,151}

This remarkable finding of the current outflow to the peripheral plasma might be of paramount importance for the ICF concept based on MPC, since the flow of the current at the larger radii impairs the implosion that compresses the liner and heats the magnetized-fuel plasma. In addition, the observed current redistribution can explain various not understood observations from other MPC experiments. These include longer implosion times and larger stagnation radius than predicted,^{149,155} the formation of helical structures of unexpectedly large pitch angle during implosion,^{149,156} the mitigation of instabilities that are stronger than expected,^{149,157,158} and the significant reduction of K-shell emission.¹⁵⁷

The evolution of the axial-magnetic-field distribution was determined using polarization spectroscopy for line emission viewed perpendicular to the axial magnetic field, combined with a laser-ablation doping technique.¹⁵¹ These measurements revealed the existence of a transition region in the axial B-field near the anode, where the uncompressed (frozen-in) B_z lines inside the metal anode converge in the plasma toward the axis farther away from the anode surface.¹⁵¹ The bending of the B-field lines that develops as the plasma implodes results in a radial B-field component that may play a role in the plasma rotation.

VIII. PLASMA ROTATION

Plasma rotation is ubiquitous both in space and laboratory plasmas. The implosion of a rotating neutral gas, even without the complication of plasma effects, already exhibits interesting phenomena.^{159,160} Imploding and compressing plasmas inherit all the complications of rotating and compressing neutral gases and are further complicated because of plasma-related effects, such as long-range electric and magnetic forces as well as various plasma-specific transport processes. The rotation effect in stabilizing the Rayleigh–Taylor instability and in avoiding radiative collapse in imploding Z-pinch plasmas was considered by Velikovich and Davis.¹⁶¹ For controlled fusion application using magnetized compressing plasma, strong rotation may enhance¹⁶² the purification of the alpha particles that can naturally occur due to collisional effects.^{163,164} Pulsed-power imploding plasma in laboratory settings can also be used to study astrophysical rotation phenomena (e.g., Refs. 8, 9, and 165–168). An important effect in laboratory setting is the mitigation of Z-pinch instabilities due to sheared flows,^{169,170} which may be related to similar physics of non-uniform distribution of angular velocity. The rotation in Z-pinch plasmas with axial magnetic fields also introduces the fundamental theoretical question of the perpendicular conductivity of rotating, magnetized, and compressing plasma, either with or without shear in the rotation.^{171,172}

These applications and fundamental questions of rotating imploding Z-pinch plasmas, particularly in the presence of an axial magnetic field, highlight the importance of detailed and reliable measurements. Recently, in the Weizmann magnetized plasma experiment (see Sec. VII), significant plasma rotation during the implosion has been observed by Cvejić *et al.*¹⁷³ The rotation was observed using chordal measurements, spatially resolved in the radial direction, in

which Doppler shifts in opposite azimuths ($-r, r$) at the same axial location were seen to have opposite signs, as schematically depicted in Fig. 22. In addition, Doppler-shifted spectral lines belonging to different charge states, that are present at different radii, allow for obtaining the rotation radial distribution without using the Abel inversion, as was done for the magnetic field radial distribution,^{129,130} discussed in Sec. VI.

Preliminary results^{173,174} show that the plasma rotation is only seen if an axial magnetic field B_{z0} is initially applied, and that the rotation direction depends on the direction of B_{z0} . It is also found that the plasma does not rotate as a rigid body, i.e., the angular velocity of the plasma has a non-uniform radial distribution that decreases inward. The magnitude of the rotation velocity $\sim 5 \times 10^6$ cm/s (see Fig. 23), being comparable to the implosion velocity, indicates that the rotation plays a significant role in both the pressure and energy balance at stagnation.

The mechanism for the rotation generation at the Weizmann MPC experiment is not clear as yet. The establishment of $E \times B$ drift that drives rotation might occur due to the Z-pinch axial E-field and the developing radial component of B in the transition region near the anode, as mentioned in Sec. VII. Another possibility may arise due to B_z and a radial electric field, which may exist in the imploding plasma, as can be seen from the generalized Ohm’s law,

$$\vec{E} = -\vec{v} \times \vec{B} + \eta \vec{j} + \frac{\vec{j} \times \vec{B}}{en_e} - \frac{\nabla p_e}{en_e}, \tag{24}$$

with the electric-field radial component

$$E_r = -\frac{j_z B_\theta}{en_e} - \frac{1}{en_e} \frac{\partial}{\partial r} p_e. \tag{25}$$

The first term on the right-hand side of Eq. (25) expresses the Hall radial electric field, and the second term gives the field due to the pressure radial gradient. Thus, detailed knowledge of the distribution of the B-field and plasma parameters is crucial for understanding the underlying physics of the imploding plasma rotation, which will be the subject of future publications.

IX. MAGNETIC-FIELD PENETRATION INTO A LOW-DENSITY PLASMA (PLASMA-OPENING SWITCH)

Plasma pushing by magnetic field pressure that, as described above, is a dominant process in Z pinches, was also expected to be the

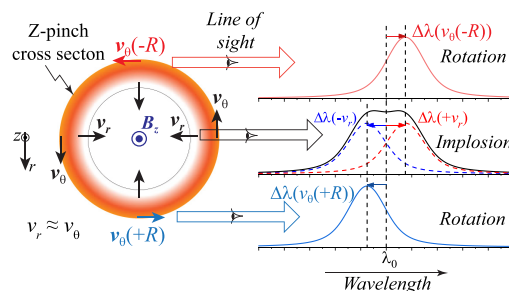


FIG. 22. Schematic of the spectroscopic measurements of rotation of the imploding plasma. Plasma rotation is demonstrated by Doppler shifts $\Delta\lambda(r)$ and $\Delta\lambda(-r)$ that have opposite signs (r is the plasma radius). v_0 and v_r are, respectively, the rotation and implosion velocities.

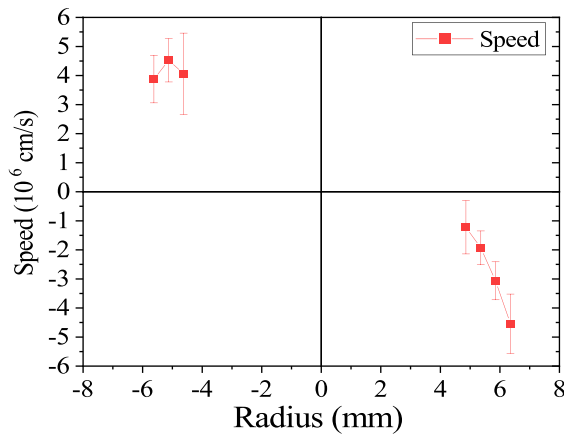


FIG. 23. Preliminary results of the rotation velocity distribution at $z = 9$ mm (where $z = 0$ mm is the anode surface) at 10 ns before stagnation (where the stagnation time is defined here as the time of smallest plasma radius).

dominant process in Plasma Opening Switches (POS).^{21,23,24,175–177} However, following indications by probe measurements,^{24,176} Zeeman-effect spectroscopic measurements with high spatial and temporal resolutions at the Weizmann Institute revealed that the magnetic field penetrates into the POS plasma in a non-diffusive manner, much faster than expected by the plasma resistivity.^{25–31,33} The fast penetration was consistent with conclusions from ion velocities measured through Doppler shifts.^{27,30,33} Observing the Zeeman effect in ionic line emission allowed for measurements that were local in three dimensions by doping the plasma using laser evaporation techniques.^{27,29}

The puzzling fast penetration of the magnetic field into the POS plasma, demonstrated unambiguously by the spectroscopic observations, was deciphered. It was shown that the Hall electric field can induce a fast magnetic field penetration if the scale of the plasma non-uniformity is smaller than the ion skin depth, as indeed often occurs in the POS low-density plasmas.^{178–185} The relation of the field penetration to the frozen-in law and to the energy balance was explained by Fruchtmann.¹⁸⁰

The mechanism of penetration is clearly demonstrated at the limit of motionless ions. With Faraday’s law, the electron momentum equation (with the Hall term, but without pressure) and Ampère’s law combined, the magnetic field is governed by the following equation:¹⁸¹

$$\frac{\partial b}{\partial t} + \frac{rb}{e\mu_0} \left\{ \frac{1}{nr^2}, b \right\} = \frac{\eta}{\mu_0} \left(\Delta b - \frac{2}{r} \frac{\partial b}{\partial r} \right). \quad (26)$$

Here, $b \equiv rB_\theta(z, r)$, $n(z, r)$ is the plasma density, η is the resistivity, μ_0 is the vacuum permeability, $\{f, g\} \equiv (\partial f / \partial z)(\partial g / \partial r) - (\partial f / \partial r)(\partial g / \partial z)$ is the Poisson brackets, and Δ is the Laplacian. The nonlinear term in the equation is due to the Hall electric field that results in a non-diffusive propagation of the magnetic field along the constant nr^2 surfaces. In deriving Eq. (26), the resistivity, for simplicity, was assumed uniform. This is justified in the POS, since the nonlinear Hall term is much larger than the resistive term, and, therefore, resistivity gradients¹²⁵ can modify the structure of the current layer, but not the velocity of field penetration. If the density only varies with r , and $\partial b / \partial z \gg \partial b / \partial r$, Eq. (26) becomes

$$\frac{\partial b}{\partial t} - \frac{r}{e\mu_0} \frac{\partial}{\partial r} \left(\frac{1}{nr^2} \right) b \frac{\partial b}{\partial z} = \frac{\eta}{\mu_0} \frac{\partial^2 b}{\partial z^2}. \quad (27)$$

This is the Burgers equation which admits traveling wave solutions in the z direction with the characteristic velocity $(r/e\mu_0)[(\partial/\partial r)(1/nr^2)]b$. Thus, either density nonuniformity or cylindrical geometry induces fast magnetic field penetration. However, the measurements showed that, unlike the simplified case of motionless ions described by Eqs. (26) and (27), both magnetic field penetration and plasma motion are significant in the POS plasma.^{25–34} In addition, they showed that the penetration was fast also when the plasma non-uniformity was small.^{29,31} These measurements have stimulated further theoretical studies that showed that the magnetic field can also penetrate into a plasma that is initially uniform,¹⁸³ and that a fine structure of the magnetic field is induced by the Hall field.^{184,185}

Further spectroscopic studies uncovered another unexpected phenomenon. It was found that ion separation accompanies the field penetration where a light-ion plasma (mainly protons) is pushed ahead, while a heavy-ion plasma (mainly carbon ions) lags behind the magnetic piston. The magnetic-field measurements allowed for demonstrating that most of the momentum imparted by the magnetic field pressure was taken by the reflected light ions, and most of the dissipated magnetic field energy was converted into kinetic energy of these ions, even though their mass is only a small part of the total plasma mass.²⁸ This discovery was then described in detail in successive studies by Arad *et al.*³⁰ and Doron *et al.*³¹ Figure 24 shows that in a specific location of the POS plasma, for $t > 200$ ns, the plasma density drops in time while the magnetic field rises. The plasma density decrease is due to the reflection of light ions, but the remaining plasma of the heavier ions, with a significant density (for $t > 250$ ns), is penetrated by the magnetic field.

Subsequent studies by Rubinstein *et al.*³³ and Doron *et al.*³⁴ provided a further striking verification of the traveling-wave-like picture

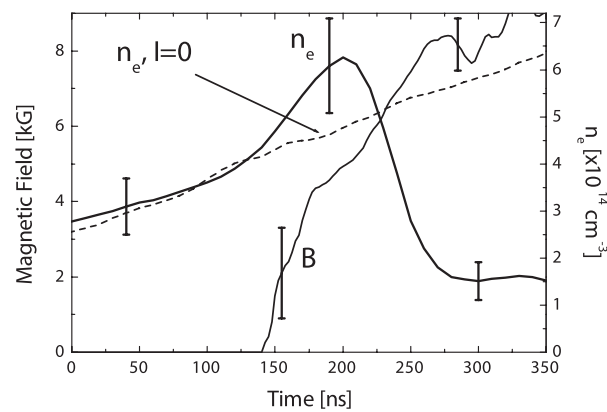


FIG. 24. The evolution of the magnetic field and the electron density. The results are from the center of the switch. The dashed curve shows the electron density evolution due to the plasma source, without the application of the current pulse. The density rise at $t > 150$ ns is due to the pushing of the light-ion plasma ahead of the propagating magnetic-field front. As the light-ion plasma leaves the observed volume ($t \sim 200$ ns), the density drops to a value that is consistent with that of the heavier-ion plasma that is penetrated by the magnetic field. Reproduced with permission from Arad *et al.*, *Phys. Plasmas* **10**, 112 (2003).²⁹ Copyright 2003 AIP Publishing.

of the magnetic field and the associated electric potential will propagate non-diffusively in the low resistivity plasma of the switch. The measured width of the propagating magnetic-field front was used to determine the plasma resistivity. Obtaining such detailed information on the structure of the propagating magnetic field required measuring the magnetic field with a high sensitivity and with a sub-mm spatial resolution. This was achieved by developing a spectroscopic method for simultaneous measurements of the time evolution of dopant ion-velocity and electron density across the magnetic-field front. In the POS low-beta plasma, the electric force that accelerates the unmagnetized ions is equal to the magnetic force on the entire plasma, which is proportional to the magnetic field gradient. Thus, the ion velocity evolution can serve as a probe for the shape of the magnetic field. Employing a laser blow-off technique, a ~ 4 -mm wide, low-density (peak ion density $< 1.5 \times 10^{13} \text{ cm}^{-3}$) dopant column was injected into the plasma. A sub-mm spatial resolution (along the line of sight) was then achieved by tracking the properties of the ions only at the center of the dopant column, as described in Refs. 33 and 34. This remarkably high spatial resolution allowed for inferring the shape of the propagating magnetic-field front with a resolution comparable to the electron skin depth ($350 \mu\text{m}$). The observed shape of the narrow current layer (the magnetic-field front) is useful for comparison with simulations that account for the complex dynamics of multi-species plasma.^{185–187}

X. FUTURE DIRECTIONS

The implementation of the method developed for measuring the ion temperature²⁰ in high-power HED experiments should be examined. Examples are the capsule experiment,⁷ the radiative-shock experiment,³⁵ and the *Hohlraum* plasma in NIF experiments.^{18,87,90} Other systems in which knowledge of the true ion temperature is crucial can also be considered.

Measurements of the time dependent current flow at different axial locations in a Z-pinch experiment may reveal interesting unpredicted phenomena, as has been seen in the Ph.D. thesis of Stollberg.¹⁸⁸ It was then shown by Ochs *et al.*¹⁸⁹ that for certain velocity profiles in the plasma, advection may result in radially outward motion of the current channel, recovering the surprising current evolution discovered in Ref. 188. Investigating such phenomena in detail, by performing even more detailed measurements of spatial **B** distributions in imploding and stagnating plasmas, and as a function of time, is expected to help understanding the interplay between the plasma flow, current flow, and plasma resistivity.

In magnetized-plasma-compression experiments, studies of the magnetic-field distributions near and farther from the electrodes, including measurements of the compression of the embedded field, should be made. Detailed spatial information on the magnetic field structure as a function of time should deepen the understanding of the plasma state, including the plasma rotation in such configurations.

Turbulence in plasmas should be studied experimentally, for example, as in Ref. 76. Measurements of the radial and axial distributions of the magnetic field and plasma flow, perhaps also by employing multiple lines of sight, are expected to be beneficial in investigating plasma turbulence in imploding-plasma experiments.

Measurements of the magnetic-field distribution in plasmas formed in high-voltage, high-current systems can be highly beneficial for determining both the diamagnetic effects of the current flow and the resistivity of plasmas (Refs. 29, 33, 110, 143). However, the

shielding of the magnetic field by the plasma¹⁴³ poses a formidable difficulty in determining the magnitude of **B** in the vacuum gaps. Determining the value of **B** produced by the current flow in high-voltage gaps requires developing methods to measure **B** in the vacuum regions in the gaps in order to avoid shielding of **B**. Also, due to the integration over space or integration over time in the measurements, the **B** field seen by the diagnostic system might not have a preferred direction in space. In these situations, the employment of the method developed for observing **B** of an arbitrary direction, utilizing no polarization properties of line emission,^{119,136,138} should be considered.

The magnetic-field measurements developed can be employed in high-power HED experiments with higher fields, using emission or absorption transitions in various spectral regions.

ACKNOWLEDGMENTS

The author is highly indebted to Ramy Doron, Eyal Kroupp, Evgeny Stambulchik, Oleg Nedostup, Vladimir Bernshtam, Marko Cvejić, Dimitry Mikitchuk, Tal Queller, Amnon Fruchtman, Vladimir Fisher, John Giuliani, Patrick Knapp, Gary Grim, Alexander Velikovich, Edmund Yu, and Nat Fisch for their substantial help in the write up of this tutorial. The author gratefully acknowledges the invaluable collaboration on the studies described in this tutorial with the colleagues and students at the Weizmann Institute, and with colleagues at worldwide institutions, in particular in those of our longstanding collaborations: Sandia National Laboratories, Cornell University, the University of Jena (Germany), U.S. Naval Research Laboratory, Princeton University, and Lawrence Livermore National Laboratory.

DATA AVAILABILITY

The data that support the findings of this study are available from the corresponding author upon reasonable request.

REFERENCES

- 1D. D. Ryutov, M. S. Derzon, and M. K. Matzen, *Rev. Mod. Phys.* **72**, 167 (2000).
- 2J. E. Bailey, G. A. Chandler, S. A. Slutz, I. Golovkin, P. W. Lake, J. J. MacFarlane, R. C. Mancini, T. J. Burris-Mog, G. Cooper, R. J. Leeper, T. A. Mehlhorn, T. C. Moore, T. J. Nash, D. S. Nielsen, C. L. Ruiz, D. G. Schroen, and W. A. Varnum, "Hot dense capsule-implosion cores produced by Z-pinch dynamic Hohlraum radiation," *Phys. Rev. Lett.* **92**, 085002 (2004).
- 3S. A. Slutz, M. C. Herrmann, R. A. Vesey, A. B. Sefkow, D. B. Sinars, D. C. Rovang, K. J. Peterson, and M. E. Cuneo, "Pulsed-power-driven cylindrical liner implosions of laser preheated fuel magnetized with an axial field," *Phys. Plasmas* **17**, 056303 (2010).
- 4M. E. Cuneo, M. C. Herrmann, D. B. Sinars, S. A. Slutz, W. A. Stygar, R. A. Vesey, A. B. Sefkow, G. A. Rochau *et al.*, "Magnetically driven implosions for inertial confinement fusion at Sandia National Laboratories," *IEEE Trans. Plasma Sci.* **40**, 3222 (2012).
- 5M. Herrmann, "Plasma physics: A promising advance in nuclear fusion," *Nature* **506**, 302 (2014).
- 6M. R. Gomez, S. A. Slutz, A. B. Sefkow, D. B. Sinars, K. D. Hahn, S. B. Hansen, E. C. Harding, P. F. Knapp, P. F. Schmit, C. A. Jennings, T. J. Awe, M. Geissel, D. C. Rovang, G. A. Chandler, G. W. Cooper, M. E. Cuneo, A. J. Harvey-Thompson, M. C. Herrmann, M. H. Hess, O. Johns, D. C. Lamppa, M. R. Martin, R. D. McBride, K. J. Peterson, J. L. Porter, G. K. Robertson, G. A. Rochau, C. L. Ruiz, M. E. Savage, I. C. Smith, W. A. Stygar, and R. A. Vesey, "Experimental demonstration of fusion-relevant conditions in magnetized liner inertial fusion," *Phys. Rev. Lett.* **113**, 155003 (2014).

- ⁷B. A. Remington, R. P. Drake, and D. D. Ryutov, "Experimental astrophysics with high power lasers and Z-pinchs," *Rev. Mod. Phys.* **78**, 755 (2006).
- ⁸P.-A. Gourdain, C. E. Seyler, L. Atayan, J. B. Greenly, D. A. Hammer, B. R. Kusse, S. A. Pikuz, W. M. Potter, P. C. Schrafel, and T. A. Shelkovenko, "The impact of Hall physics on magnetized high energy density plasma jets," *Phys. Plasmas* **21**, 056307 (2014).
- ⁹S. V. Lebedev, A. Frank, and D. D. Ryutov, "Exploring astrophysics-relevant magnetohydrodynamics with pulsed-power laboratory facilities," *Rev. Mod. Phys.* **91**, 025002 (2019).
- ¹⁰E. Kroupp, D. Osin, A. Starobinets, V. I. Fisher, V. Bernshtam, Y. Maron, I. Uschmann, E. Forster, A. Fisher, and C. Deeney, "Ion kinetic-energy measurements and energy balance in a z-pinch plasma at stagnation," *Phys. Rev. Lett.* **98**, 115001 (2007).
- ¹¹E. Kroupp, D. Osin, A. Starobinets, V. Fisher, V. Bernshtam, L. Weingarten, Y. Maron, I. Uschmann, E. Förster, A. Fisher, M. E. Cuneo, C. Deeney, and J. L. Giuliani, "Ion temperature and hydrodynamic-energy measurements in a Z-pinch plasma at stagnation," *Phys. Rev. Lett.* **107**, 105001 (2011).
- ¹²B. Jones, C. Deeney, C. A. Coverdale, P. D. LePell, J. L. McKenney, J. P. Apruzese, J. W. Thornhill, K. G. Whitney, R. W. Clark, A. L. Velikovich, J. Davids, Y. Maron, V. Kantsyrev, A. Safronova, and V. I. Oreshkin, "K-shell radiation physics in low- to moderate-atomic-number z-pinch plasmas on the Z accelerator," *J. Quant. Spectrosc. Radiat. Transfer* **99**, 341–348 (2006).
- ¹³C. A. Coverdale, C. Deeney, B. Jones, J. W. Thornhill, K. G. Whitney, A. L. Velikovich, R. W. Clark, Y. K. Chong, J. P. Apruzese, J. Davis, and P. D. LePell, "Scaling of K-shell emission from Z-pinchs: Z to ZR," *IEEE Trans. Plasma Sci.* **35**(3), 582–591 (2007).
- ¹⁴B. Jones, C. A. Jennings, D. C. Lamppa, S. B. Hansen, A. J. Harvey-Thompson, D. J. Ampleford, M. E. Cuneo, T. Strizic, D. Johnson, M. C. Jones, N. W. Moore, T. M. Flanagan, J. L. McKenney, E. M. Waisman, C. A. Coverdale, M. Krishnan, P. L. Coleman, K. W. Elliott, R. E. Madden, J. Thompson, A. Bixler, J. W. Thornhill, J. L. Giuliani, Y. K. Chong, A. L. Velikovich, A. Dasgupta, and J. P. Apruzese, "A renewed capability for gas puff science on Sandia's Z machine," *IEEE Trans. Plasma Sci.* **42**(5), 1145–1152 (2014).
- ¹⁵D. J. Ampleford, B. Jones, C. A. Jennings, S. B. Hansen, M. E. Cuneo, A. J. Harvey-Thompson, G. A. Rochau, C. A. Coverdale, A. R. Laspe, T. M. Flanagan *et al.*, "Contrasting physics in wire array Z-pinch sources of 1-20 keV emission on the Z facility," *Phys. Plasmas* **21**, 056708 (2014).
- ¹⁶J. L. Giuliani and R. J. Comisso, "A review of the gas-puff Z-pinch as an X-ray and neutron source," *IEEE Trans. Plasma Sci.* **43**(8), 2385 (2015).
- ¹⁷C. A. Coverdale, C. Deeney, A. L. Velikovich, J. Davis, R. W. Clark, Y. K. Chong, J. Chittenden, S. Chantrenne, C. L. Ruiz, G. W. Cooper, A. J. Nelson, J. Franklin, P. D. LePell, J. P. Apruzese, J. Levine, and J. Banister, "Deuterium gas-puff Z-pinch implosions on the Z accelerator," *Phys. Plasmas* **14**, 056309 (2007).
- ¹⁸J. Lindl, "Development of the indirect-drive approach to inertial confinement fusion and the target physics basis for ignition and gain," *Phys. Plasmas* **2**, 3933 (1995).
- ¹⁹R. S. Craxton, K. S. Anderson, T. R. Boehly, V. N. Goncharov, D. R. Harding, J. P. Knauer, R. L. McCrory, P. W. McKenty, D. D. Meyerhofer, J. F. Myatt, A. J. Schmitt, J. D. Sethian, R. W. Short, S. Skupsky, W. Theobald, W. L. Kruer, K. Tanaka, R. Betti, T. J. B. Collins, J. A. Delettrez, S. X. Hu, J. A. Marozas, A. V. Maximov, D. T. Michel, P. B. Radha, S. P. Regan, T. C. Sangster, W. Seka, A. A. Solodov, J. M. Soures, C. Stoeckl, and J. D. Zuegel, "Direct-drive inertial confinement fusion: A review," *Phys. Plasmas* **22**, 110501 (2015).
- ²⁰D. Alumat, E. Kroupp, E. Sambulchik, A. Starobinets, I. Uschmann, and Y. Maron, "Determination of the ion temperature in a high-energy-density plasma using the Stark effect," *Phys. Rev. Lett.* **122**, 095001 (2019).
- ²¹W. Mendel, Jr. and S. A. Goldstein, *J. Appl. Phys.* **48**, 1004 (1977).
- ²²G. Cooperstein and P. F. Ottinger, "Special issue on fast opening vacuum switches for high-power inductive energy storage," *IEEE Trans. Plasma Sci.* **15**(6) (1987); and references therein.
- ²³R. W. Stinnett, D. H. Mcdaniel, G. E. Rochau, W. B. Moore, E. W. Gray, T. J. Renk, H. N. Woodall, T. W. Hussey, S. S. Payne, R. J. Comisso, J. M. Grossmann, D. D. Hinshelwood, R. A. Meger, J. M. Neri, W. F. Oliphant, P. F. Ottinger, and B. V. Weber, "Plasma opening switch development for the particle beam fusion accelerator II (PBFA II)," *IEEE Trans. Plasma Sci.* **15**, 557 (1987).
- ²⁴V. Weber, R. J. Comisso, R. A. Meger, J. M. Neri, W. F. Oliphant, and P. F. Ottinger, *Appl. Phys. Lett.* **45**, 1043 (1984).
- ²⁵M. Sarfaty, Y. Maron, Ya. E. Krasik, A. Weingarten, R. Arad, R. Shpitalnik, A. Fruchtmann, and S. Alexiou, *Phys. Plasmas* **2**, 2122 (1995).
- ²⁶M. Sarfaty, R. Shpitalnik, R. Arad, A. Weingarten, Ya. E. Krasik, A. Fruchtmann, and Y. Maron, *Phys. Plasmas* **2**, 2583 (1995).
- ²⁷R. Shpitalnik, A. Weingarten, K. Gomberoff, Y. Krasik, and Y. Maron, *Phys. Plasmas* **5**, 792 (1998).
- ²⁸A. Weingarten, R. Arad, Y. Maron, and A. Fruchtmann, *Phys. Rev. Lett.* **87**, 115004 (2001).
- ²⁹R. Arad, K. Tsigutkin, Y. Maron, A. Fruchtmann, and J. D. Huba, "Observation of faster-than-diffusion magnetic field penetration into a plasma," *Phys. Plasmas* **10**, 112 (2003).
- ³⁰R. Arad, K. Tsigutkin, Y. Maron, and A. Fruchtmann, *Phys. Plasmas* **11**, 4515 (2004).
- ³¹R. Doron, R. Arad, K. Tsigutkin, D. Osin, A. Weingarten, A. Starobinets, V. A. Bernshtam, E. Stambulchik, Yu. V. Ralchenko, Y. Maron, A. Fruchtmann, A. Fisher, J. D. Huba, and M. Roth, *Phys. Plasmas* **11**, 2411 (2004).
- ³²K. Tsigutkin, R. Doron, E. Stambulchik, V. Bernshtam, Y. Maron, A. Fruchtmann, and R. J. Comisso, *Phys. Rev. E* **76**, 046401 (2007).
- ³³B. Rubinstein, R. Doron, Y. Maron, A. Fruchtmann, and T. A. Mehlhorn, *Phys. Plasmas* **23**, 040703 (2016).
- ³⁴R. Doron, B. Rubinstein, J. Citrin, R. Arad, Y. Maron, A. Fruchtmann, H. R. Strauss, and T. A. Mehlhorn, *Phys. Plasmas* **23**, 122126 (2016).
- ³⁵G. A. Rochau, J. E. Bailey, Y. Maron, G. A. Chandler, G. S. Dunham, D. V. Fisher, V. I. Fisher, R. W. Lemke, J. MacFarlane, K. J. Peterson, D. G. Schroen, S. A. Slutz, and E. Stambulchik, "Radiating shock measurements in the Z-pinch dynamic Hohlraum," *Phys. Rev. Lett.* **100**, 125004 (2008).
- ³⁶D. A. Hammer and B. R. Kusse, in *Proceedings of the 7th International Conference on Dense Z-Pinchs, Alexandria, VA* (AIP, Melville, NY, 2009).
- ³⁷N. Qi, S. V. Rocco, J. Engelbrecht, E. S. Lavine, P. de Grouchy, J. T. Banasek, L. Atayan, T. Byvank, W. M. Potter, J. B. Greenly, D. A. Hammer, B. R. Kusse, S. A. Pikuz, T. A. Shelkovenko, E. Kroupp, A. Fisher, and Y. Maron, "Study of triple Ar gas puff Z-pinchs on 0.9-MA, 200-ns COBRA," *IEEE Trans. Plasma Sci.* **46**, 3864–3870 (2018).
- ³⁸S. A. Slutz, "Scaling of magnetized inertial fusion with drive current rise-time," *Phys. Plasmas* **25**, 082707 (2018).
- ³⁹S. A. Slutz and R. A. Vesey, *Phys. Rev. Lett.* **108**, 025003 (2012).
- ⁴⁰V. I. Fisher, D. V. Fisher, and Y. Maron, "Radiation transport and density effects in plasmas," *High Energy Density Phys.* **3**, 283 (2007).
- ⁴¹H. A. Scott and S. B. Hansen, "Advances in NLTE modeling for integrated simulations," *High Energy Density Phys.* **6**(1), 39–47 (2010).
- ⁴²J. W. Thornhill, J. L. Giuliani, Y. K. Chong, A. L. Velikovich, A. Dasgupta, J. P. Apruzese, B. Jones, D. J. Ampleford, C. A. Coverdale, C. A. Jennings, E. M. Waisman, D. C. Lamppa, J. L. McKenney, M. E. Cuneo, M. Krishnan, P. L. Coleman, R. E. Madden, and K. W. Elliott, "Two-dimensional radiation MHD modeling assessment of designs for argon gas puff distributions for future experiments on the refurbished Z machine," *High Energy Density Phys.* **8**(3), 197 (2012).
- ⁴³P. Chittenden and C. A. Jennings, "Development of instabilities in wire-array Z-pinchs," *Phys. Rev. Lett.* **101**, 055005 (2008).
- ⁴⁴C. A. Jennings, M. E. Cuneo, E. M. Waisman, D. B. Sinars, D. J. Ampleford, G. R. Bennett, W. A. Stygar, and J. P. Chittenden, *Phys. Plasmas* **17**, 092703 (2010).
- ⁴⁵K. L. Wong, P. R. Springer, J. H. Hammer, C. A. Iglesias, A. L. Osterheld, M. E. Foord, H. C. Bruns, J. A. Emig, and C. Deeney, *Phys. Rev. Lett.* **80**, 2334 (1998).
- ⁴⁶E. J. Yadlowsky, F. Barakat, E. P. Carlson, R. C. Hazelton, M. Keitz, C. C. K. B. H. Failor, J. S. Levine, Y. Song, B. L. Whitten, C. R. Coverdale *et al.*, *J. Appl. Phys.* **92**, 3458 (2002).
- ⁴⁷M. G. Haines, P. D. LePell, C. A. Coverdale, B. Jones, C. Deeney, and J. P. Apruzese, "Ion viscous heating in a magnetohydrodynamically unstable Z-pinch at over 2×10^9 Kelvin," *Phys. Rev. Lett.* **96**, 075003 (2006).
- ⁴⁸Y. Fan, L. Zheng-Hong, Q. Yi, J. Shu-Qing, X. Fei-Biao, Y. Jian-Lun, X. Rong-Kun, and J. Yong-Jie, "Spatially-resolved spectroscopic diagnosing of aluminum wire array Z-pinch plasmas on QiangGuang-I facility," *Chin. Phys. B* **19**(7), 075204 (2010).

- ⁴⁹J. F. Seely, "Density-sensitive dielectronic satellite lines in microballon neon spectra," *Phys. Rev. Lett.* **42**, 1606 (1979).
- ⁵⁰E. Kroupp, A. Starobinets, E. Klodzh, Yu. V. Ralchenko, Y. Maron, I. N. Bogatu, and A. Fisher, "Investigation of Ne IX and Ne X line emission from dense plasma using Ross-filter systems," *J. Appl. Phys.* **92**, 4947–4951 (2002).
- ⁵¹Y. V. Ralchenko and Y. Maron, "Accelerated recombination due to resonant deexcitation of metastable states," *J. Quant. Spectrosc. Radiat. Transfer* **71**, 609–621 (2001).
- ⁵²R. H. Lovberg, R. A. Riley, and J. S. Shlachter, "Instability heating of the HDZP," in *3rd International Conference Dense Z-Pinches, London, UK 1993*, edited by M. Haines, A. Knight, R. H. Lovberg, R. A. Riley, and J. S. Shlachter, [AIP Conf. Proc. **299**, 51 (1994)].
- ⁵³L. I. Rudakov and R. N. Sudan, "MHD turbulence in radiating intense Z-pinches," *Phys. Rep.* **283**, 253 (1997).
- ⁵⁴L. I. Rudakov, A. L. Velikovich, J. Davis, J. W. Thornhill, J. L. Giuliani, Jr., and C. Deeney, "Buoyant magnetic flux tubes enhance radiation in Z-pinches," *Phys. Rev. Lett.* **84**, 3326 (2000).
- ⁵⁵L. Velikovich, L. I. Rudakov, J. Davis, J. W. Thornhill, J. L. Giuliani, Jr., and C. Deeney, "Model of enhanced energy deposition in a Z-pinch plasma," *Phys. Plasmas* **7**, 3265 (2000).
- ⁵⁶K. G. Whitney, J. W. Thornhill, J. P. Apruzese, and J. Davis, "Enhanced energy coupling and x-ray emission in Z-pinch plasma implosions," *Phys. Plasmas* **11**, 3700 (2004).
- ⁵⁷M. G. Haines, "A review of the dense Z-pinch," *Plasma Phys. Controlled Fusion* **53**, 093001 (2011).
- ⁵⁸J. D. Sethian, A. E. Robson, K. A. Gerber, and A. W. DeSilva, "Enhanced stability and neutron production in a dense Z-pinch plasma formed from a frozen deuterium fiber," *Phys. Rev. Lett.* **59**, 892 (1987).
- ⁵⁹M. G. Haines, "An analytic model of radiative collapse of a Z pinch," *Plasma Phys. Controlled Fusion* **31**, 759 (1989).
- ⁶⁰A. E. Robson, "Radiative collapse of a z pinch in hydrogen and helium," *Phys. Fluids B* **1**, 1834 (1989).
- ⁶¹W. H. Bennett, *Phys. Rev.* **45**, 890 (1934).
- ⁶²P. Chittenden, S. V. Lebedev, C. A. Jennings, S. N. Bland, and A. Ciardi, *Plasma Phys. Controlled Fusion* **46**, B457 (2004).
- ⁶³C. Deeney, P. D. LePell, B. H. Failor, S. L. Wong, J. P. Apruzese, K. G. Whitney, J. W. Thornhill, J. Davis, E. Yadlowsky, R. C. Hazelton, J. J. Moschella, T. Nash, and N. Loter, *Phys. Rev. E* **51**, 4823 (1995).
- ⁶⁴Y. Maron, A. Starobinets, V. I. Fisher, E. Kroupp, D. Osin, A. Fisher, C. Deeney, C. A. Coverdale, P. D. Lepell, E. P. Yu, C. Jennings, M. E. Cuneo, M. C. Herrmann, J. L. Porter, T. A. Mehlhorn, and J. P. Apruzese, "Pressure and energy balance of stagnating plasmas in z-pinch experiments: Implications to current flow at stagnation," *Phys. Rev. Lett.* **111**, 035001 (2013).
- ⁶⁵C. A. Coverdale, M. E. Cuneo, C. Jennings, B. Jones, C. Deeney, P. D. LePell, and Y. Maron, "Nested array dynamics from Ni-clad Ti-Al wire array Z-pinches," in *38th IEEE International Conference on Plasma Science (ICOPS), Abstracts of Contributed Papers, Chicago, USA (IEEE, New York, 2011)*, p. 1.
- ⁶⁶G. A. Rochau, J. E. Bailey, and Y. Maron, "Applied spectroscopy in pulsed power plasmas," *Phys. Plasmas* **17**, 055501 (2010), and references therein.
- ⁶⁷S. L. Gavriluk and R. Saurel, *J. Fluid Mech.* **575**, 495 (2007); A. L. Velikovich, C. Huete, and J. G. Wouchuk, *Phys. Rev. E* **85**, 016301 (2012).
- ⁶⁸P. Yu, M. E. Cuneo, M. P. Desjarlais, R. W. Lemke, D. B. Sinars, T. A. Hail, E. M. Waisman, G. R. Bennett, C. A. Jennings, T. A. Mehlhorn, T. A. Brunner, H. L. Hanshaw, J. L. Porter, W. A. Stygar, and L. I. Rudakov, "Three-dimensional effects in trailing mass in the wire-array Z pinch," *Phys. Plasmas* **15**, 056301 (2008).
- ⁶⁹J. L. Giuliani, J. W. Thornhill, E. Kroupp, D. Osin, Y. Maron, A. Dasgupta, A. L. Velikovich, J. P. Apruzese, Y. K. Chong, A. Starobinets, V. Fisher, Yu. Zarnitsky, V. Bernshtam, A. Fisher, T. A. Mehlhorn, and C. Deeney, "Effective vs ion thermal temperatures in the Weizmann Ne Z-pinch: Modeling and stagnation physics," *Phys. Plasmas* **21**, 031209 (2014).
- ⁷⁰J. W. Thornhill, J. P. Apruzese, J. Davis, R. W. Clark, A. L. Velikovich, J. L. Giuliani, Y. K. Chong, K. G. Whitney, C. Deeney, C. A. Coverdale, and F. L. Cochran, "An efficient tabulated collisional radiative equilibrium radiation transport model suitable for multidimensional hydrodynamics calculations," *Phys. Plasmas* **8**, 3480–3489 (2001).
- ⁷¹E. P. Yu, A. L. Velikovich, and Y. Maron, "Application of one-dimensional stagnation solutions to three-dimensional simulation of compact wire array in absence of radiation," *Phys. Plasmas* **21**, 082703 (2014).
- ⁷²E. Kroupp, L. Gregorian, G. Davara, A. Starobinets, E. Stambulchik, Y. Maron, Yu. Ralchenko, and S. Alexiou, "Spectroscopic investigation of the particle density and motion in an imploding z-pinch plasma," in *Atomic Processes in Plasmas*, edited by J. D. Gillaspay, J. J. Curry, and W. L. Wiese (AIP, 2007) [AIP Conf. Proc. **926**, 4–7 (2007)].
- ⁷³S. Davidovits and N. J. Fisch, "Sudden viscous dissipation of compressing turbulence," *Phys. Rev. Lett.* **116**, 105004 (2016).
- ⁷⁴S. Davidovits and N. J. Fisch, "A lower bound on adiabatic heating of compressed turbulence for simulation and model validation," *Astrophys. J.* **838**, 118 (2017).
- ⁷⁵P. F. Hopkins, "A model for (non-lognormal) density distributions in isothermal turbulence," *Mon. Not. R. Astron. Soc.* **430**, 1880 (2013).
- ⁷⁶E. Kroupp, E. Stambulchik, A. Starobinets, D. Osin, V. I. Fisher, D. Alumot, Y. Maron, S. Davidovits, N. J. Fisch, and A. Fruchtman, "Turbulent stagnation in a Z-pinch plasma," *Phys. Rev. E* **97**, 013202 (2018).
- ⁷⁷M. E. Savage, K. R. LeChien, M. R. Lopez, B. S. Stoltzfus, W. A. Stygar, D. S. Artery, J. A. Lott, and P. A. Corcoran, in *Proceedings of the 18th International Pulsed Power Conference, Chicago, IL (IEEE, New York, 2011)*, pp. 983–990.
- ⁷⁸S. Davidovits and N. J. Fisch, "Bulk hydrodynamic stability and turbulent saturation in compressing hot spots," *Phys. Plasmas* **25**, 042703 (2018).
- ⁷⁹S. Davidovits and N. J. Fisch, "Modeling turbulent energy behavior and sudden viscous dissipation in compressing plasma turbulence," *Phys. Plasmas* **24**, 122311 (2017).
- ⁸⁰S. Davidovits and N. J. Fisch, "Compressing turbulence and sudden viscous dissipation with compression-dependent ionization state," *Phys. Rev. E* **94**, 053206 (2016).
- ⁸¹B. Robertson and P. Goldreich, "Adiabatic heating of contracting turbulent fluids," *Astrophys. J. Lett.* **750**, L31 (2012).
- ⁸²B. G. Elmegreen, "Variations in stellar clustering with environment: Dispersed star formation and the origin of faint fuzzies," *Astrophys. J.* **672**, 1006 (2008).
- ⁸³P. Padoan and A. Nordlund, "The stellar initial mass function from turbulent fragmentation," *Astrophys. J.* **576**, 870 (2002).
- ⁸⁴J. Ballesteros-Paredes, A. Gazol, J. Kim, R. S. Klessen, A.-K. Jappsen, and E. Tejero, "The mass spectra of cores in turbulent molecular clouds and implications for the initial mass function," *Astrophys. J.* **637**, 384 (2006).
- ⁸⁵P. Hennebelle and G. Chabrier, "Analytical theory for the initial mass function: CO clumps and prestellar cores," *Astrophys. J.* **684**, 395 (2008).
- ⁸⁶G. Kritsuk, C. T. Lee, and M. L. Norman, "A supersonic turbulence origin of Larson's laws," *Mon. Not. R. Astron. Soc.* **436**, 3247 (2013).
- ⁸⁷L. Kritcher, R. Town, D. Bradley, D. Clark, B. Spears, O. Jones, S. Haan, P. T. Springer, J. Lindl, R. H. H. Scott, D. Callahan, M. J. Edwards, and O. L. Landen, "Metrics for long wavelength asymmetries in inertial confinement fusion implosions on the National Ignition Facility," *Phys. Plasmas* **21**, 042708 (2014).
- ⁸⁸S. Davidovits and N. J. Fisch, "Understanding turbulence in compressing plasma in as a quasi-EOS," *Phys. Plasmas* **26**, 062709 (2019).
- ⁸⁹S. Davidovits and N. J. Fisch, "Viscous dissipation in two-dimensional compression of turbulence," *Phys. Plasmas* **26**, 082702 (2019).
- ⁹⁰L. C. Jarrott, B. Bachmann, T. Ma, L. R. Benedetti, F. E. Field, E. P. Hartouni, R. Hatarik, N. Izumi, S. F. Khan, L. Landen, S. R. Nagel, R. Nora, A. Pak, J. L. Peterson, M. B. Schneider, P. T. Springer, and P. K. Patel, "Thermal temperature measurements of inertial fusion implosions," *Phys. Rev. Lett.* **121**, 085001 (2018).
- ⁹¹P. F. Knapp, D. B. Sinars, and K. D. Hahn, "Diagnosing suprathreshold on populations in Z-pinch plasmas using fusion neutron spectra," *Phys. Plasmas* **20**, 062701 (2013).
- ⁹²R. Hatarik, R. C. Nora, B. K. Spears, M. J. Eckart, G. P. Grim, E. P. Hartouni, A. S. Moore, and D. J. Schlossberg, "Using multiple neutron time of flight detectors to determine the hot spot velocity," *Rev. Sci. Instrum.* **89**, 101138 (2018).
- ⁹³D. H. Munro, "Interpreting inertial fusion neutron spectra," *Nucl. Fusion* **56**, 036001 (2016).

- ⁹⁴D. H. Munro, J. E. Field, R. Hatarik, J. L. Peterson, E. P. Hartouni, B. K. Spears, and J. D. Kilkenny, "Impact of temperature-velocity distribution on fusion neutron peak shape," *Phys. Plasmas* **24**, 056301 (2017).
- ⁹⁵H. R. Griem, *Spectral Line Broadening by Plasmas* (Academic, New York, 1974).
- ⁹⁶S. H. Glenzer and R. Redmer, "X-ray Thomson scattering in high energy density plasmas," *Rev. Mod. Phys.* **81**, 1625 (2009).
- ⁹⁷J. Holtzmark, "Über die Verbreiterung von Spektrallinien," *Ann. Phys.* **363**, 577 (1919).
- ⁹⁸V. Demura, "Physical models of plasma microfield," *Int. J. Spectrosc.* **2010**, 1.
- ⁹⁹E. Stambulchik and Y. Maron, "A study of ion-dynamics and correlation effects for spectral line broadening in plasma: K-shell lines," *J. Quant. Spectrosc. Radiat. Transfer* **99**, 730–749 (2006).
- ¹⁰⁰E. Stambulchik and Y. Maron, "Quasicontiguous frequency-fluctuation model for calculation of hydrogen and hydrogenlike Stark-broadened line shapes in plasmas," *Phys. Rev. E* **87**, 053108 (2013).
- ¹⁰¹V. Fisher, private communication (July 2015).
- ¹⁰²S. N. Bland, D. J. Ampleford, S. C. Bott, A. Guite, G. N. Hall, S. M. Hardy, S. V. Lebedev, P. Shardlow, A. Harvey-Thompson, F. Suzuki, and K. H. Kwek, "Use of Faraday probing to estimate current distribution in wire array z-pinch," *Rev. Sci. Instrum.* **77**, 10E315 (2006).
- ¹⁰³V. V. Ivanov, A. A. Anderson, D. Papp, B. R. Talbot, J. P. Chittenden, N. Niasse, and I. A. Begishev, "UV laser-probing diagnostics for the dense Z pinch," *IEEE Trans. Plasma Sci.* **42**(5), 1153–1161 (2014).
- ¹⁰⁴V. V. Ivanov, A. A. Anderson, D. Papp, A. L. Astanovitskiy, B. R. Talbot, J. P. Chittenden, and N. Niasse, *Phys. Rev. E* **88**, 013108 (2013).
- ¹⁰⁵M. Borghesi, A. Schiavi, D. H. Campbell, M. G. Haines, O. Willi, A. J. MacKinnon, L. A. Gizzi, M. Galimberti, R. J. Clarke, and H. Ruhl, "Proton imaging: A diagnostic for inertial confinement fusion/fast ignitor studies," *Plasma Phys. Controlled Fusion* **43**, A267 (2001).
- ¹⁰⁶C. K. Li, F. H. Séguin, J. A. Frenje, J. R. Rygg, R. D. Petrasso, R. P. J. Town, P. A. Amendt, S. P. Hatchett, O. L. Landen, A. J. Mackinnon, P. K. Patel, V. A. Smalyuk, T. C. Sangster, and J. P. Knauer, "Measuring E and B fields in laser-produced plasmas with monoenergetic proton radiography," *Phys. Rev. Lett.* **97**, 135003 (2006).
- ¹⁰⁷P. M. Nilson, L. Willingale, M. C. Kaluza, C. Kamperidis, S. Minardi, M. S. Wei, P. Fernandes, M. Notley, S. Bandyopadhyay, M. Sherlock, R. J. Kingham, M. Tatarakis, Z. Najmudin, W. Rozmus, R. G. Evans, M. G. Haines, A. E. Dangor, and K. Krushelnick, "Magnetic reconnection and plasma dynamics in two-beam laser-solid interactions," *Phys. Rev. Lett.* **97**, 255001 (2006).
- ¹⁰⁸N. L. Kugland, D. D. Ryutov, C. Plechaty, J. S. Ross, and H.-S. Park, "Invited article: Relation between electric and magnetic field structures and their proton-beam images," *Rev. Sci. Instrum.* **83**, 101301 (2012).
- ¹⁰⁹D. Mariscal, C. McGuffey, J. Valenzuela, M. S. Wei, J. P. Chittenden, N. Niasse, R. Presura, S. Haque, M. Wallace, A. Arias, A. Covington, H. Sawada, P. Wiewior, and F. N. Beg, "Measurement of pulsed-power-driven magnetic fields via proton deflectometry," *Appl. Phys. Lett.* **105**, 224103 (2014).
- ¹¹⁰Y. Maron, E. Sarid, E. Nahshoni, and O. Zahavi, "Time dependent spectroscopic observation of the magnetic field in a high-power-diode plasma," *Phys. Rev. A* **39**, 5856 (1989).
- ¹¹¹T. M. Antonsen and E. Ott, *Phys. Fluids* **19**, 52 (1976).
- ¹¹²Y. Maron, M. D. Coleman, D. A. Hammer, and H. S. Peng, "Measurements of the electric field distribution in high-power diodes," *Phys. Rev. Lett.* **57**, 699 (1986).
- ¹¹³Y. Maron, M. D. Coleman, D. A. Hammer, and H. S. Peng, "Experimental determination of the electric field and charge distribution in magnetically insulated diodes," *Phys. Rev. A* **36**, 2818 (1987).
- ¹¹⁴J. Bailey, A. B. Filuk, A. L. Carlson, D. J. Johnson, P. Lake, E. J. McGuire, T. A. Mehlhorn, T. D. Pointon, T. J. Renk, W. A. Stygar, and Y. Maron, "Measurements of acceleration gap dynamics on a 20 TW applied-magnetic-field ion diode," *Phys. Rev. Lett.* **74**, 1771 (1995).
- ¹¹⁵E. Stambulchik, Y. Maron, J. E. Bailey, and M. E. Cuneo, "Polarization properties of ion-excitation mechanisms in high voltage gaps," *Phys. Rev. A* **65**, 52726 (2002).
- ¹¹⁶J. E. Bailey, A. B. Filuk, A. L. Carlson, D. J. Johnson, P. Lake, E. J. McGuire, T. A. Mehlhorn, T. D. Pointon, T. J. Rank, W. A. Stygar, Y. Maron, and E. Stambulchik, "Basic and applied atomic spectroscopy in high-field ion diode acceleration gaps," *Laser Part. Beams* **14**, 543 (1996).
- ¹¹⁷F. C. Jahoda, F. L. Ribe, and G. A. Sawyer, "Zeeman-effect magnetic field measurement of a high-temperature plasma," *Phys. Rev.* **131**, 24 (1963).
- ¹¹⁸J. Peacock and B. A. Norton, "Measurement of megagauss magnetic fields in a plasma focus device," *Phys. Rev. A* **11**, 2142 (1975).
- ¹¹⁹R. Doron, D. Mikitchuk, C. Stollberg, G. Rosenzweig, E. Stambulchik, E. Kroupp, Y. Maron, and D. A. Hammer, "Determination of magnetic fields based on the Zeeman effect in regimes inaccessible by Zeeman-splitting spectroscopy," *High Energy Density Phys.* **10**, 56 (2014).
- ¹²⁰G. Davara, L. Gregorian, E. Kroupp, and Y. Maron, "Spectroscopic determination of the magnetic-field distribution in an imploding plasma," *Phys. Plasmas* **5**, 1068 (1998).
- ¹²¹A. N. Tikhonov and A. A. Samarski, *Partial Differential Equations of Mathematical Physics* (Holden-Day, San Francisco, CA, 1964).
- ¹²²L. Gregorian, V. A. Bernshtam, E. Kroupp, G. Davara, and Y. Maron, "Use of emission-line intensities for a self-consistent determination of the particle densities in a transient plasma," *Phys. Rev. E* **67**, 016404 (2003).
- ¹²³L. Gregorian, E. Kroupp, G. Davara, A. Starobinets, V. I. Fisher, V. A. Bernshtam, Y. V. Ralchenko, Y. Maron, A. Fisher, and D. H. H. Hoffmann, "Electron-temperature and energy-flow history in an imploding plasma," *Phys. Rev. E* **71**, 056402 (2005).
- ¹²⁴L. Gregorian, E. Kroupp, G. Davara, V. I. Fisher, A. Starobinets, V. A. Bernshtam, A. Fisher, and Y. Maron, "Electron density and ionization dynamics in an imploding Z-pinch plasma," *Phys. Plasmas* **12**, 092704 (2005).
- ¹²⁵P.-A. Gourdain, M. B. Adams, J. R. Davies, and C. E. Seyler, *Phys. Plasmas* **24**, 102712 (2017).
- ¹²⁶M. E. Foord, Y. Maron, G. Davara, L. Gregorian, and A. Fisher, "Particle velocity distributions and ionization processes in a gas-puff Z pinch," *Phys. Rev. Lett.* **72**, 3827–3830 (1994).
- ¹²⁷P. Golingo, U. Shumlak, and D. J. D. Hartog, "Note: Zeeman splitting measurements in a high-temperature plasma," *Rev. Sci. Instrum.* **81**, 126104 (2010).
- ¹²⁸M. R. Gomez, S. B. Hansen, K. J. Peterson, D. E. Bliss, A. L. Carlson, D. C. Lamppa, D. G. Schroen, and G. A. Rochau, "Magnetic field measurements via visible spectroscopy on the Z machine," *Rev. Sci. Instrum.* **85**, 11E609 (2014).
- ¹²⁹G. Rosenzweig, E. Kroupp, A. Fisher, and Y. Maron, "Measurements of the spatial magnetic field distribution in a z-pinch plasma throughout the stagnation process," *J. Instrum.* **12**, P09004 (2017).
- ¹³⁰G. Rosenzweig, E. Kroupp, T. Queller, A. Starobinets, Y. Maron, V. Tangri, J. Giuliani, and A. Fruchtman, "Local measurements of the spatial magnetic field distribution in a Z-pinch plasma during and near stagnation using polarization spectroscopy," *Phys. Plasmas* **27**, 022705 (2020).
- ¹³¹J. F. Seely, U. Feldman, N. R. Sheeley, Jr., S. Suckewer, and A. M. Title, "Magnetic field measurements based on the Zeeman splitting of forbidden transitions," *Rev. Sci. Instrum.* **56**, 855 (1985).
- ¹³²T. Shikama and P. M. Bellan, "Development of a polarization resolved spectroscopic diagnostic for measurements of the vector magnetic field in the Caltech coaxial magnetized plasma jet experiment," *Rev. Sci. Instrum.* **84**, 023507 (2013).
- ¹³³D. Mikitchuk, M. Cvejić, R. Doron, E. Kroupp, C. Stollberg, Y. Maron, A. L. Velikovich, N. D. Ouart, J. L. Giuliani, T. A. Mehlhorn, E. P. Yu, and A. Fruchtman, "Effects of a preembedded axial magnetic field on the current distribution in a Z-pinch implosion," *Phys. Rev. Lett.* **122**, 045001 (2019).
- ¹³⁴D. Osin, E. Kroupp, A. Starobinets, G. Rosenzweig, D. Alumot, Y. Maron, A. Fisher, E. Yu, J. L. Giuliani, and C. Deeney, "Evolution of MHD instabilities in plasma imploding under magnetic field," *IEEE Trans. Plasma Sci.* **39**, 2392–2393 (2011).
- ¹³⁵V. Tangri, private communication (December 2019).
- ¹³⁶E. Stambulchik, K. Tsigitkin, and Y. Maron, "Spectroscopic method for measuring plasma magnetic fields having arbitrary distributions of direction and amplitude," *Phys. Rev. Lett.* **98**, 225001 (2007).
- ¹³⁷E. Stambulchik and Y. Maron, "Effect of high-n and continuum eigenstates on the Stark effect of resonance lines of atoms and ions," *Phys. Rev. A* **56**, 2713 (1997).
- ¹³⁸S. Tessarin, D. Mikitchuk, R. Doron, E. Stambulchik, E. Kroupp, Y. Maron, D. A. Hammer, V. L. Jacobs, J. F. Seely, B. V. Oliver, and A. Fisher, "Beyond Zeeman spectroscopy: Magnetic-field diagnostics with Stark-dominated line shapes," *Phys. Plasmas* **18**, 093301 (2011).

- ¹³⁹K. D. Hahn, N. Bruner, M. D. Johnston, B. V. Oliver, T. J. Webb, D. R. Welch, S. R. Cordova, I. Crotch, R. E. Gignac, J. J. Leckbee, I. Molina, S. Portillo, J. R. Threadgold, and D. Ziska, *IEEE Trans. Plasma Sci.* **38**, 2652 (2010).
- ¹⁴⁰M. D. Johnston, S. G. Patel, R. E. Falcon, K. Cartwright, M. L. Kiefer, M. E. Cuneo, and Y. Maron, "Measuring plasma formation, field strength, and current loss in pulsed power diodes," Sandia National Laboratories Report No. SAND2017-12565 (2017).
- ¹⁴¹B. V. Oliver, K. Hahn, M. D. Johnston, and S. Portillo, *Acta Phys. Pol., A* **115**, 1044 (2009).
- ¹⁴²S. G. Patel, M. D. Johnston, T. J. Webb, N. L. Bennett, D. R. Welch, R. M. Gilgenbach, M. E. Cuneo, M. L. Kiefer, J. J. Leckbee, M. G. Mazarakis, D. J. Muron, T. J. Renk, S. C. Simpson, R. Doron, S. Biswas, D. Mikitchuk, and Y. Maron, "Zeeman spectroscopy as a method for determining the magnetic field distribution in self-magnetic-pinch diodes," *Rev. Sci. Instrum.* **89**, 10D123 (2018).
- ¹⁴³S. Biswas, M. D. Johnston, R. Doron, D. Mikitchuk, Y. Maron, S. G. Patel, M. L. Kiefer, and M. E. Cuneo, "Shielding of the azimuthal magnetic field by the anode plasma in a relativistic self-magnetic-pinch diode," *Phys. Plasmas* **25**, 113102 (2018).
- ¹⁴⁴F. S. Felber, F. J. Wessel, N. C. Wild, H. U. Rahman, A. Fisher, C. M. Fowler, M. A. Liberman, and A. L. Velikovich, *J. Appl. Phys.* **64**(8), 3831–3844 (1988).
- ¹⁴⁵F. S. Felber, M. M. Malley, F. J. Wessel, M. K. Matzen, M. A. Palmer, R. B. Spielman, M. A. Liberman, and A. L. Velikovich, *Phys. Fluids* **31**(7), 2053–2056 (1988).
- ¹⁴⁶R. K. Appartaim and A. E. Dangor, *J. Appl. Phys.* **84**(8), 4170–4175 (1998).
- ¹⁴⁷S. A. Chaikovsky, A. Y. Labetsky, V. I. Oreshkin, A. V. Shishlov, R. B. Baksht, A. V. Fedunin, and A. G. Roussikh, *Laser Part. Beams* **21**, 255–264 (2003).
- ¹⁴⁸G. G. Zvakishvili, K. N. Mitrofanov, E. V. Grabovskii, and G. M. Oleinik, *Plasma Phys. Rep.* **31**, 652–664 (2005).
- ¹⁴⁹D. Mikitchuk, C. Stollberg, R. Doron, E. Kroupp, Y. Maron, H. R. Strauss, A. L. Velikovich, and J. L. Giuliani, "Mitigation of instabilities in a Z-pinch plasma by a preembedded axial magnetic field," *IEEE Trans. Plasma Sci.* **42**, 2524–2525 (2014).
- ¹⁵⁰D. A. Yager-Elorriaga, Y. Y. Lau, P. Zhang, P. C. Campbell, A. M. Steiner, N. M. Jordan, R. D. McBride, and R. M. Gilgenbach, "Evolution of sausage and helical modes in magnetized thin-foil cylindrical liners driven by a Z-pinch," *Phys. Plasmas* **25**, 056307 (2018).
- ¹⁵¹D. Mikitchuk, *Investigation of the Compression of Magnetized Plasma and Magnetic Flux*, Springer Theses Series (Springer, 2019).
- ¹⁵²A. L. Velikovich, N. D. Ouart, J. L. Giuliani, R. B. Baksht, A. G. Roussikh, V. I. Oreshkin, D. Mikitchuk, M. Cvejić, R. Doron, E. Kroup, and Y. Maron, "Force-free current flow in Z pinches imploded in axial magnetic field," in IEEE International Conference on Plasma Science (ICOPS) (2017).
- ¹⁵³C. E. Seyler, M. R. Martin, and N. D. Hamlin, *Phys. Plasmas* **25**, 062711 (2018).
- ¹⁵⁴A. B. Sefkow, *Bull. Am. Phys. Soc.* **61**, 373 (2016).
- ¹⁵⁵G. Roussikh, A. S. Zhigalin, V. I. Oreshkin, V. Frolova, A. L. Velikovich, G. Yu. Yushkov, and R. B. Baksht, "Effect of the axial magnetic field on a metallic gas-puff pinch implosion," *Phys. Plasmas* **23**(6), 063502 (2016).
- ¹⁵⁶T. J. Awe, R. D. McBride, C. A. Jennings, D. C. Lamppa, M. R. Martin, D. C. Rovang, S. A. Slutz, M. E. Cuneo, A. C. Owen, D. B. Sinars, K. Tomlinson, M. R. Gomez, S. B. Hansen, M. C. Herrmann, J. L. McKenney, C. Nakhleh, G. K. Robertson, G. A. Rochau, M. E. Savage, D. G. Schroen, and W. A. Stygar, *Phys. Rev. Lett.* **111**, 235005 (2013).
- ¹⁵⁷V. Shishlov, R. B. Baksht, S. A. Chaikovsky, A. V. Fedunin, F. I. Fursov, V. A. Kokshenev, N. E. Kurmaev, A. Yu. Labetsky, V. I. Oreshkin, N. A. Ratakhin, A. G. Roussikh, and S. V. Shlykhtun, *Laser Phys.* **16**(1), 183–193 (2006).
- ¹⁵⁸N. Qi, P. de Grouchy, P. C. Schrafel, L. Atoyian, W. M. Potter, A. D. Cahill, P.-A. Gourdain, J. B. Greenly, D. A. Hammer, C. L. Hoyt, B. R. Kusse, S. A. Pikuz, and T. A. Shelkovenko, *AIP Conf. Proc.* **1639**, 51 (2014).
- ¹⁵⁹V. I. Geyko and N. J. Fisch, "Reduced compressibility and an inverse problem for a spinning gas," *Phys. Rev. Lett.* **110**, 150604 (2013).
- ¹⁶⁰V. I. Geyko and N. J. Fisch, "Piezothermal effect in a spinning gas," *Phys. Rev. E* **94**, 042113 (2016).
- ¹⁶¹A. L. Velikovich and J. Davis, "Implosions, equilibria, and stability of rotating, radiating Z-pinch plasmas," *Phys. Plasmas* **2**, 4513 (1995).
- ¹⁶²E. J. Kolmes, I. E. Ochs, and N. J. Fisch, "Strategies for advantageous differential transport of ions in magnetic fusion devices," *Phys. Plasmas* **25**, 032508 (2018).
- ¹⁶³I. E. Ochs and N. J. Fisch, "Favorable collisional demixing of ash and fuel in magnetized inertial fusion," *Phys. Rev. Lett.* **121**, 235002 (2018).
- ¹⁶⁴I. E. Ochs and N. J. Fisch, "Anisotropy-driven collisional separation of impurities in magnetized compressing and expanding cylindrical plasmas," *Phys. Plasmas* **25**, 122306 (2018).
- ¹⁶⁵D. J. Ampleford, S. V. Lebedev, A. Ciardi, S. N. Bland, S. C. Bott, G. N. Hall, N. Naz, C. A. Jennings, M. Sherlock, J. P. Chittenden, J. B. A. Palmer, A. Frank, and E. Blackman, "Supersonic radiatively cooled rotating flows and jets in the laboratory," *Phys. Rev. Lett.* **100**, 035001 (2008).
- ¹⁶⁶M. J. Bennett, S. V. Lebedev, G. N. Hall, L. Suttle, G. Burdiak, F. Suzuki-Vidal, J. Hare, G. Swadling, S. Patankar, M. Bocchi, J. P. Chittenden, R. Smith, A. Frank, E. Blackman, R. P. Drake, C. A. Jennings, C. E. Seyler, and B. R. Kusse, "Applied axial magnetic field effects on laboratory plasma jets: Density hollowing, field compression, and azimuthal rotation," *Phys. Plasmas* **24**, 122701 (2017).
- ¹⁶⁷T. Byvank, J. T. Banasek, W. M. Potter, J. B. Greenly, C. E. Seyler, and B. R. Kusse, "Sustained neutron production from a sheared-flow stabilized Z-pinch," *Phys. Rev. Lett.* **122**, 135001 (2019).
- ¹⁶⁸S. V. Lebedev, A. Ciardi, D. J. Ampleford, S. N. Bland, S. C. Bott, J. P. Chittenden, G. N. Hall, J. Rapley, C. A. Jennings, A. Frank, E. G. Blackman, and T. Lery, "Magnetic tower outflows from a radial wire array Z-pinch," *Mon. Not. R. Astron. Soc.* **361**, 97–108 (2005).
- ¹⁶⁹B. Hassam, "Nonlinear stabilization of the Rayleigh–Taylor instability by external velocity shear," *Phys. Fluids B* **4**, 485 (1992).
- ¹⁷⁰Y. Zhang, U. Shumlak, B. A. Nelson, R. P. Golingo, T. R. Weber, A. D. Stepanov, E. L. Claveau, E. G. Forbes, Z. T. Draper, J. M. Mitrani, H. S. McLean, K. K. Tummel, D. P. Higginson, and C. M. Cooper, "Sustained neutron production from a sheared-flow stabilized Z-pinch," *Phys. Rev. Lett.* **122**, 135001 (2019).
- ¹⁷¹J. M. Rax, E. J. Kolmes, I. E. Ochs, N. J. Fisch, and R. Gueroult, "Nonlinear ohmic dissipation in axisymmetric DC and RF driven rotating plasmas," *Phys. Plasmas* **26**, 012303 (2019).
- ¹⁷²E. J. Kolmes, I. E. Ochs, M. E. Mlodik, J. M. Rax, R. Gueroult, and N. J. Fisch, "Radial current and rotation profile tailoring in highly ionized linear plasma devices," *Phys. Plasmas* **26**, 082309 (2019).
- ¹⁷³M. Cvejić, D. Mikitchuk, E. Kroupp, R. Doron, Y. Maron, and U. Shumlak, "Ion velocities measurements in Z-pinch with pre-embedded axial magnetic field," in 37th Annual Conference and Workshop on IVS-IPSTA 2019, Haifa, 3 September (2019).
- ¹⁷⁴M. Cvejić, D. Mikitchuk, P. Sharma, E. Kroupp, R. Doron, Y. Maron, A. L. Velikovich, and A. Fruchtman, "Ion velocities measurements in Z-pinch with pre-embedded axial magnetic field" (unpublished).
- ¹⁷⁵P. F. Ottinger, S. A. Goldstein, and R. A. Meger, *J. Appl. Phys.* **56**, 774 (1984).
- ¹⁷⁶D. Hinshelwood, J. R. Boller, R. J. Comisso, G. Cooperstein, R. A. Meger, J. M. Neri, P. F. Ottinger, and B. V. Weber, *Appl. Phys. Lett.* **49**, 1635 (1986).
- ¹⁷⁷C. W. Mendel, Jr., M. E. Savage, D. M. Zagar, W. W. Simpson, T. W. Grasser, and J. P. Quintenz, *J. Appl. Phys.* **71**, 3731 (1992).
- ¹⁷⁸A. S. Kingsep, Y. V. Mokhov, and K. V. Chukbar, *Sov. J. Plasma Phys.* **10**, 495 (1984).
- ¹⁷⁹V. Gordeev, A. S. Kingsep, and L. I. Rudakov, *Phys. Rep.* **243**, 215 (1994).
- ¹⁸⁰A. Fruchtman, *Phys. Fluids B* **3**, 1908 (1991); *Phys. Rev. A* **45**, 3938 (1992).
- ¹⁸¹A. Fruchtman and K. Gomberoff, *Phys. Fluids* **5**, 2371 (1993).
- ¹⁸²J. D. Huba, J. M. Grossmann, and P. F. Ottinger, *Phys. Plasmas* **1**, 3444 (1994).
- ¹⁸³A. Fruchtman and L. I. Rudakov, *Phys. Rev. Lett.* **69**, 2070 (1992); *Phys. Rev. E* **50**, 2997 (1994).
- ¹⁸⁴S. B. Swanekamp, J. M. Grossmann, A. Fruchtman, B. V. Oliver, and P. F. Ottinger, *Phys. Plasmas* **3**, 3556 (1996).
- ¹⁸⁵A. Richardson, J. Angus, S. Swanekamp, P. F. Ottinger, and J. Schumer, *IEEE Trans. Plasma Sci.* **42**, 2552 (2014).
- ¹⁸⁶V. Gordeev, *Plasma Phys. Rep.* **27**, 659 (2001) [*Fiz. Plazmy* **27**, 700 (2001)].
- ¹⁸⁷H. R. Strauss, R. Doron, R. Arad, B. Rubinstein, Y. Maron, and A. Fruchtman, *Phys. Plasmas* **14**, 053504 (2007).
- ¹⁸⁸C. Stollberg, "Investigation of a small-scale self-compressing plasma column," Ph.D. thesis (Weizmann Institute of Science, 2019).
- ¹⁸⁹I. E. Ochs, C. Stollberg, E. Kroupp, Y. Maron, A. Fruchtman, E. J. Kolmes, M. E. Mlodik, and N. J. Fisch, "Current channel evolution in ideal Z pinch for general velocity profiles," *Phys. Plasmas* **26**, 122706 (2019).